Impacts of oxidizer concentration and fuel composition on near-source aerosol emissions from lignocellulosic biomass and constituent burning

Luke P. McLaughlin, Erica L. Belmont

PII: S0021-8502(21)00556-5

DOI: https://doi.org/10.1016/j.jaerosci.2021.105825

Reference: AS 105825

To appear in: *Journal of Aerosol Science*

Received Date: 26 April 2021

Revised Date: 12 May 2021

Accepted Date: 13 May 2021

Please cite this article as: McLaughlin LP, Belmont EL, Impacts of oxidizer concentration and fuel composition on near-source aerosol emissions from lignocellulosic biomass and constituent burning, *Journal of Aerosol Science* (2021), doi: https://doi.org/10.1016/j.jaerosci.2021.105825.

Impacts of Oxidizer Concentration and Fuel Composition on Near-Source Aerosol Emissions from Lignocellulosic Biomass and Constituent Burning

Luke P. McLaughlin, Erica L. Belmont[*]

Department of Mechanical Engineering, The University of Wyoming, Laramie, Wyoming, United States

[*]*Corresponding Author: 1000 E. University Ave. Laramie, WY, 82071, ebelmont@uwyo.edu, +1-307-766-6073*

Abstract: Biomass burning (BB), a multi-step process including drying, devolatilization, and oxidation of volatiles and char, is a globally occurring phenomenon that is understood to produce significant quantities of aerosols that have a broad range of local and global effects on humans and the environment. Quantities and properties of BB-derived aerosols are difficult to predict due to the complex nature of BB. Near-source conditions, such as oxygen availability and fuel composition, have been identified as influential factors in the properties of aerosol emissions. This work examined the total and size-resolved number and mass aerosol emission factors from dry, pulverized lignocellulosic biomass and its major constituents under laboratory burning conditions to understand the influence of oxygen level and fuel composition on near-source aerosol production. Lignocellulosic biomass and major constituents, including hemicellulose (xylan), cellulose and lignin, were pyrolyzed and combusted in inert and oxidative environments at varying oxygen levels, and the aerosol particle emissions were characterized in terms of size and quantity at a fixed dilution temperature. Fuel mass and fuel heating rate were varied to assess the sensitivity of results to these factors. A previously developed summative model to predict near-source BB aerosol emissions was also tested. Results showed that the total number and mass aerosol emissions decreased with increased oxygen levels. Nucleation mode particles

dominated the number emissions in both inert and oxidative environments, but larger aerosol sizes were observed in the oxidative environment. Aerosol particle coagulation and growth were observed at larger fuel masses, indicated by a significant decrease in the total number emission factors in both inert and oxidative environments, while the total mass emission factor only slightly decreased and increased in inert and oxidative environments, respectively. The size of aerosols formed was found to positively correlate with absolute fuel consumption rate, and the effects of oxidation through combustion chemistry and thermal feedback were explored. Good agreement between the simulated and measured number emission factors for pinewood was observed in both the inert and oxidative reaction environments over the range of tested fuel masses. Simulated and measured mass emission factors showed good agreement in the oxidative environment and poorer agreement in the inert environment. Reasons for this discrepancy were explored and the importance of constituent surrogate selection is highlighted.

Keywords: Biomass Emissions; Aerosol; Pyrolysis; Oxidation; Coagulation; Fuel Mass

1. Introduction

Biomass burning (BB) is a global phenomenon that produces significant quantities of aerosol particles and gases which have local and global implications such as negative health effects and radiative forcing (Andreae & Merlet, 2001; Bond et al., 2004; Chen et al., 2017; Reid, Eck, et al., 2005). These emissions from BB can have particularly negative health impacts for nearby persons and influence near-source heat transfer, and some of these emissions escape the fire zone and evolve into atmospherically sensed aerosols (Muala et al., 2015; Pardo et al., 2020; Sutherland & Khanna, 1991; Ward & Radke, 1993). The human and environmental impacts of BB emissions vary widely and many are closely related to the physical properties of the aerosols, including aerosol size and quantity (Chen et al., 2017; Reid, Koppmann, et al., 2005). BB is naturally complex and consists of several steps including drying, devolatilization, and oxidation of volatiles and char (Fang et al., 2014). BB-derived primary organic aerosols (POA) are aerosols directly released from the fire event (Bond et al., 2004; Zhou et al., 2017) and BB accounts for about 75% of global POA production, but POA formation is difficult to predict due to the complex nature of BB (Cao et al., 2019; Jolleys et al., 2014; May et al., 2013). BB aerosol emissions generally consist of about 50-60% organic carbon and about 5-10% black carbon (Reid, Koppmann, et al., 2005), but aerosol composition and other properties, such as size distribution, are influenced by fuel type, combustion efficiency, and environmental conditions (Collier et al., 2016; Liu et al., 2014; Petters et al., 2009).

Among the complicating factors in predicting BB-derived OA is variability in conditions near the fire, such as fuel mass, fuel consumption rate and combustion chemistry (Jolleys et al., 2012). Fuel mass, or fuel load, was investigated in previous works for its effect on particulate mass emission factors (EF) and it was suggested that the influence of fuel mass on particulate mass EF

was minimal (Grandesso et al., 2011; Shen et al., 2013). Shen et al. burned corn straw in an indoor cookstove and found that the particulate mass, organic carbon, and elemental carbon EF were independent of the fuel mass between 275-1100 g. Grandesso et al. burned loblolly pine in a closed chamber under conditions simulating a forest prescribed burn and found that the total particulate mass EF were independent of a 1-10 kg fuel mass. Fuel consumption rate, defined as the change in fuel mass with respect to burning time, has been linearly correlated to fire radiative power (FRP) (Wooster et al., 2005), and FRP has also been linearly correlated to aerosol mass emission rates (Ichoku & Kaufman, 2005). These findings suggest that the fuel consumption rate influences the rate of aerosol emissions generated during BB. Additionally, higher emissions concentrations and larger fire areas have also been shown to increase aerosol coagulation and mean aerosol diameter (Hodshire et al., 2019; Ramnarine et al., 2019; Sakamoto et al., 2016). Aerosol coagulation is understood to occur shortly after emission and most rapidly in the initial plume evolution (Formenti et al., 2003; Hodshire et al., 2019), and coagulation rate has been found to be proportional to the square of particle number concentration (Hodshire et al., 2019). Further complicating the prediction of OA emissions, combustion chemistry entails complex oxidation reactions involving particle precursor species. These reactions are influenced by the combustion zone temperature and oxygen availability, and these reactions determine the chemical makeup and volatility of the produced species (Fitzpatrick et al., 2007; Kroll & Seinfeld, 2008; Orasche et al., 2013; Reid, Koppmann, et al., 2005). Combustion products at low temperatures will include holocellulose and lignin pyrolysis products such as hydroxyacetaldehyde, acetic acid, levoglucosan, furans, guiacols, syringols, and phenols, which are semi-volatile with a propensity to condense into aerosols (Fitzpatrick et al., 2007; Orasche et al., 2013). At higher temperatures, the formation of polycyclic aromatic hydrocarbons (PAH) and

oxygenated PAH are favored (Fitzpatrick et al., 2007; Orasche et al., 2013), and these species form incipient particles which then act as nucleation sites for adsorption of semi-volatile species and aerosol growth. These results suggest that variability in oxidative environments near a fire may significantly influence not only the chemical composition, but also the number and size of aerosol emissions.

As a result of uncertainties associated with naturally occurring BB events and the associated difficulty of OA emissions prediction, research needs have been identified in the literature and guided the study presented herein. The influence of oxygen availability during combustion on OA emissions has been identified as important to more closely scrutinize due to variable oxygen availability during BB (Jolleys et al., 2014). Additionally, the influence of variability in fuel properties for different fuel types on OA emissions has been identified to be important and in need of further study (Jolleys et al., 2014). In this work, the influences of oxygen availability during combustion and fuel composition on the size and quantity of aerosols produced from pulverized pinewood and the major lignocellulosic biomass constituents – hemicellulose (xylan), cellulose, and lignin – were investigated in a controlled laboratory setting to obtain new insights into mechanisms influencing POA formation in biomass burning events. Sample fuel mass and fuel heating rate were varied to assess the sensitivity of the results to fuel mass and fuel consumption rates. The effect of emissions dilution ratio shortly downstream of the source was also investigated. Fuels were pyrolyzed and oxidized over a range of ambient oxygen levels and fuel masses, and size-resolved aerosol emissions were quantified over the time of fuel consumption. The aerosol emissions measurements from the major lignocellulosic biomass constituents were then used to further test a previously developed summative model to predict near-source lignocellulosic biomass emissions from measurement of constituent-derived aerosols

and the mass fraction of each constituent in the lignocellulosic biomass. This work expands the application of that model to both inert and oxidative environments over a range of fuel masses and examines the highlights and shortcomings of the model.

2. Methods

2.1 Biomass and Constituents

Lodgepole pinewood sourced from the Medicine Bow National Forest near Centennial, WY was chosen as the lignocellulosic biomass for examination in this study. The pinewood was ground and sieved to a particle size range of 75-106 μm, and then dried at 100 °C for 24 h and stored in a desiccator until used in experiments. The major constituents of lignocellulosic biomass – cellulose, hemicellulose, and lignin – were tested in this study using Avicel (Sigma Aldrich, PH-101), xylan (Sigma Aldrich, from Beechwood), and Kraft lignin (Storaenso, from pine and Nordic spruce) with a 97% dry lignin content, respectively, as representative compounds. The pinewood and lignocellulosic biomass constituents were characterized for moisture content (MC), volatile content (VC), fixed carbon content (FC) and ash content (AC) using the KAR procedure (López-García et al., 2013), a slightly modified ASTM D7582 proximate analysis method. Dry-basis results from the KAR procedure are shown in Table 1. The pinewood sample was also characterized for constituent make-up, including cellulose, hemicellulose, and lignin contents, at the National Renewable Energy Laboratory (NREL) in Golden CO, and results are also shown in Table 1. The galactan, arabinan, and mannan constituents of the pinewood were added to the hemicellulose mass fraction. Inorganic content, proteins, and extractives make up the remaining biomass content, and production of aerosols from these components was assumed to be negligible because of their relatively small fractions as compared to the major components. As a result, those components were assigned zero aerosol emissions in the modeling performed

in this study. Other biomass types may contain greater inorganic content and produce greater fractions of inorganic aerosols (May et al., 2014), and inorganic content of the fuel and its role in aerosol formation warrants further investigation for those fuels.

Table 1. Proximate and constituent analyses of the pinewood and major lignocellulosic biomass constituents on a dry basis. Constituent analysis for pinewood was performed by NREL.

	VC (wt%)	FC (wt%)	AC (wt%)	Lignin (wt%)	Cellulose (wt%)	Hemicellulose (wt%)
Lodgepole pine	85.58 ± 1.14	11.10 ± 1.08	3.32 ± 0.26	28.30	35.76	20.73
Cellulose	94.80 ± 0.24	4.46 ± 0.32	0.74 ± 0.08	n/a	100.0	n/a
Hemicellulose	77.44 ± 0.43	19.32 ± 0.14	3.24 ± 0.30	n/a	n/a	100.0
Lignin	64.66 ± 0.70	33.70 ± 1.22	1.64 ± 0.53	100.0	n/a	n/a

2.2 Experimental Platform

Figure 1 shows a schematic of the experimental setup used in this work to pyrolyze or oxidize the fuel samples, and then to dilute and sample the resultant aerosol emissions. Pinewood and the lignocellulosic biomass constituents were thermally degraded in inert and oxidative environments using a TA Instruments Q500 Thermogravimetric Analyzer (TGA) fitted with an evolved gas analysis (EGA) furnace and 100 μL alumina sample pans. The EGA furnace is quartz-lined and thus inert to devolatilization products produced within the furnace, which allows for accurate sampling of the aerosol emissions. Ultra-high purity nitrogen (N_2, 99.999%) and ultra-high purity oxygen (O_2, 99.999%) were mixed and flowed over the sample at a total flow rate of 90 mL/min while ultra-high purity nitrogen (N_2, 99.999%) was flowed through the balance and into the furnace at 10 mL/min. Temperature measurements within the EGA furnace

were achieved via a K-type thermocouple adjacent to the sample, and the thermocouple was calibrated via a Curie point calibration.

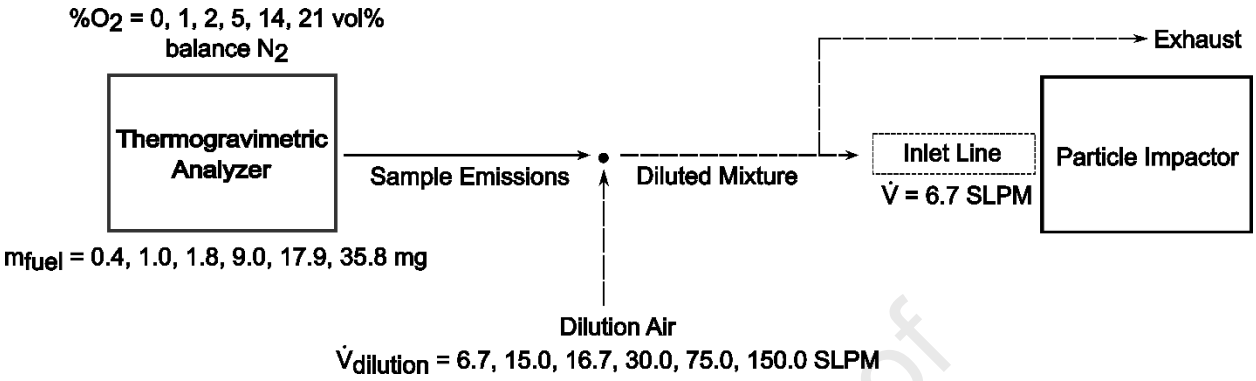

Figure 1. Schematic of pyrolysis/oxidation and aerosol sampling platform, including a thermogravimetric analyzer (TGA) coupled to a particle impactor for aerosol characterization. Sample emissions from the TGA are mixed with dilution air to achieve the desired fuel mass-to-dilution flow rate (m_{fuel}: $\dot{V}_{dilution}$) ratio. Dashed lines are either ¼" or 1" diameter stainless steel tubing for the small and large sampling apparatuses, respectively.

Each biomass or constituent sample, for every test performed in this study, was heated to 100 °C in a selected reaction environment gas and held isothermal for 10 minutes to remove any moisture from the sample. Samples were then heated at a heating rate of 20 °C/min for most tests, except heating rate tests which were performed at 10 °C/min and 50 °C/min, to 800 °C and held isothermal until the samples were fully oxidized or pyrolyzed and the aerosol formation event ended.

Upon exiting the TGA, emissions were diluted with dry lab air at 293 K to simulate BB emissions mixing into the surrounding environment and to prevent saturation of the aerosol sampling instrument detectors. Diluted emissions were then transported through tubing indicated by the solid and dashed lines in Fig. 1. Two versions of the experimental setup were used to

enable testing of variable fuel mass while minimizing changes in fuel mass-to-dilution ratios: a small sampling apparatus that utilized ¼" diameter stainless steel tubing, and a large sampling apparatus that utilized 1" diameter stainless steel tubing. Following dilution, 6.7 SLPM (standard liters per minute at 273 K and 1 atm) of the diluted emissions stream was drawn by a vacuum pump through a 1.5 m sample line to a Dekati High-Temperature Electrical Low-Pressure Impactor (HT-ELPI) for real-time aerosol size and number measurements. The HT-ELPI has 14 stages for aerosol detection with a sensing range of 10 nm to 10 μm. Three replicates were performed for each sample in the variable oxidation level experiments and variable fuel mass experiments, and trial-to-trial uncertainty was quantified using Student's t-test with a 95% confidence interval. Additionally, to ensure that the aerosols detected during experiments were not artifacts of the experimental technique, several checks including zero-air checks, blank sample runs, and HEPA filter tests were performed, and more details regarding the checks can be found in McLaughlin & Belmont (2021).

2.3 Experimental Test Plan

In this work, the reaction environment oxygen level was varied to investigate its effect on the aerosol number and mass emissions from pyrolysis and oxidation of pulverized pinewood and the major lignocellulosic biomass constituents. Fuel mass and fuel heating rate were varied to investigate the sensitivity of the results to variable fuel mass and fuel consumption rate. Fuel consumption rate is defined as the change in fuel mass with respect to time in this work. Tables 2 and 3 summarize the details of each pinewood and constituent experiment that was performed and the associated naming convention for results plot legends. First, the reaction environment oxygen level was varied at a fixed fuel mass of 0.4 mg and fixed heating rate of 20 °C/min to investigate the influence of O_2 levels on size-resolved and total aerosol emission factors from

pinewood and constituents. The reaction environment consisted of either 0, 1, 2, 5, 14, or 21 vol% O_2 balanced by N_2 for pinewood, while constituents were only tested at 0 and 21 vol% O_2. While 0 vol% O_2 environments likely do not occur in terrestrial fires, tests in inert environments were used to gain insights into the role of reaction environment oxygen level and combustion chemistry on aerosol emissions. During these tests, the TGA flow rate and dilution flow rate were fixed at 0.1 SLPM and 6.7 SLPM, respectively, resulting in a dilution ratio of 1:67 and a fuel mass (m_{fuel}) to dilution flow rate ($\dot{V}_{dilution}$) ratio, m_{fuel}: $\dot{V}_{dilution}$, of 1:16.75. The small sampling apparatus was used for the variable oxygen level tests which resulted in a total residence time, from when the aerosols exited the EGA furnace until the start of aerosol detection, of approximately 2.3 s.

Next, fuel mass was varied at a fixed heating rate of 20 °C/min to investigate the influence of fuel sample size on total and size-resolved aerosol emission factors from pinewood and constituents in 0 and 21 vol% O_2. Fuel masses of 0.4, 1.0, 1.8, 9.0, 17.9, and 35.8 mg were tested for pinewood, while constituents were only investigated at fuel masses of 0.4, 17.9, and 35.8 mg. The TGA environment gas flow rate was fixed at 0.1 SLPM and the dilution flow rate was 6.7, 15.0, 16.8, 30.0, 75.0, or 150.0 SLPM to limit the variation of m_{fuel}: $\dot{V}_{dilution}$, and resulted in m_{fuel}: $\dot{V}_{dilution}$ ratios of 1:16.75 (100% m_{fuel}: $\dot{V}_{dilution}$), 1:8.38 (50% m_{fuel}: $\dot{V}_{dilution}$), and 1:4.19 (25% m_{fuel}: $\dot{V}_{dilution}$). The small and large sampling apparatuses were utilized to achieve the desired m_{fuel}: $\dot{V}_{dilution}$ while maintaining comparable residence times and protecting the TGA from back-pressurization. These apparatus configurations resulted in a minimum residence time of 2.3 s and a maximum residence time of 2.7 s over the range of tests that were performed.

Additionally, utilizing the large sampling apparatus, the influence of fuel consumption rate on aerosol emissions was investigated in 0 vol% O_2 at a fuel mass of 17.9 mg and 50% m_{fuel}: $\dot{V}_{dilution}$ by applying heating rates of 10 °C/min and 50 °C/min to the pinewood and comparing the size-resolved and total aerosol number and mass emission factors to results at 20 °C/min.

Although oxidation level, fuel mass, and fuel consumption rate were the primary variables investigated in this study, several checks were performed to ensure that the resulting number and mass emission factors were not significantly influenced by variable m_{fuel}: $\dot{V}_{dilution}$, residence time, or sampling apparatus size. The influence of m_{fuel}: $\dot{V}_{dilution}$ was investigated by comparing the total number and mass emission factors determined for pinewood at each m_{fuel}: $\dot{V}_{dilution}$ value (25%, 50%, and 100%). To test whether different residence times and sample apparatus sizes significantly influenced the measured aerosol emissions, tests of a 1.0 mg pinewood sample in 21 vol% O_2 with a 100% m_{fuel}: $\dot{V}_{dilution}$ were carried out at two different residence times of 2.3 s and 2.5 s, utilizing the small and large sampling apparatuses respectively, and residence time was added to the small sampling apparatus with additional tubing length to achieve a total residence time of 2.5 s. The resulting total number and mass emission factors were compared.

Table 2. Experimental test matrix for the pinewood and constituent samples, where S = small sampling apparatus, L = large sampling apparatus, t_{res} = added residence time, -H = 10 °C/min heating rate, +H = 50 °C/min heating rate, x = pinewood sample only, and y = pinewood and constituent samples. Greyed out lines indicate no tests were performed at those conditions, and all tests were performed at 20 °C/min unless otherwise denoted.

Fuel Mass (mg)	**m_{fuel}: $\dot{V}_{dilution}$**	**0%**				**1%**		**2%**		**5%**		**14%**		**21%**		
		S	**L**	**L**	**L +**	**S**	**L**	**S**	**L**	**S**	**L**	**S**	**L**	**S**	**L**	**S + t_{res}**

				-H	H											
0.4	100%	y				x		x		x		x		y		
	50%															
	25%															
1.0	100%													x	x	x
	50%														x	
	25%															
1.8	100%														x	
	50%														x	
	25%															
9.0	100%														x	
	50%															
	25%															
17.9	100%															
	50%		y	x	x										y	
	25%														x	
35.8	100%															
	50%															
	25%		y												y	

Table 3. Variable mass test naming convention for pinewood, where S = small sampling apparatus, L = large sampling apparatus, t_{res} = added residence time, -H = 10 °C/min heating rate, and +H = 50 °C/min heating rate. All tests were performed at 20 °C/min unless otherwise denoted.

m_{fuel}: $\dot{V}_{dilution}$ (%)	vol% O_2	Sampling Apparatus Size	Name
100%	0%	S	100% smPY
	21%	S	100% smOX
		S + t_{res}	100% smOX + t_{res}
		L	100% lgOX
50%	0%	L	50% lgPY
		L - H	50% lgPY - H
		L + H	50% lgPY + H
	21%	L	50% lgOX
25%	0%	L	25% lgPY
	21%	L	25% lgOX

2.4 Emission Factors

Aerosol number and size measurements were determined by the HT-ELPI, which senses the charge carried by aerosols as a signal in femto-amperes and translates the signal to real-time measurements of particle number concentration at each of the 14 impactor stages, or size bins. The mean particle number concentration of each size bin measured over a small time-period, N_i, is then translated to a number emission factor, $EF_{N,i}$, which is the number of particles collected by an individual impactor stage over an applied time period divided by the starting fuel mass. The total number emission factor, $EF_{N,tot}$, is defined as the sum of the size-resolved number emission factors as

$$EF_{N,tot} = \sum_{i=1}^{n} EF_{N,i} = \sum_{i=1}^{n} \frac{N_i \cdot \dot{V} \cdot \Delta t}{m_{fuel}} \quad (1)$$

where Δt is the applied time period, m_{fuel} is the starting fuel sample mass, $\dot{V}$ is the volumetric flow rate of the diluted emission stream and n is the number of included stages in the HT-ELPI. Similarly, the mass emission factor, defined as the mass of aerosols formed over a given time period and divided by the starting fuel mass, was determined from the corresponding number emission factors and aerodynamic bin diameters by

$$EF_{M,tot} = \sum_{i=1}^{n} EF_{M,i} = \sum_{i=1}^{n} \rho \cdot V_i \cdot EF_{N,i} \quad (2)$$

where ρ is the particle density, assumed to be 1 g·cm^{-3} because the aerodynamic diameter was used to determine mass, and V_i is the particle volume corresponding to the aerodynamic diameter, D_i, of the particle. In this work, the number and mass emission factors were determined over the duration of the pyrolysis and oxidation experiments.

In addition to experimental measurements, emission factors were simulated using a previously developed model for pyrolysis emission factors (McLaughlin & Belmont, 2021). In the study described herein, this model was applied to the simulation of emission factors for pyrolysis and oxidation of pinewood with varied fuel mass to evaluate its utility for these conditions. The model utilizes a superposition technique in which the measured emission factors, both size-resolved and total, from the major lignocellulosic biomass constituents during pyrolysis and oxidation at various fuel masses are combined with their corresponding mass fractions in the biomass to predict the emission factors from biomass. Given the fuel preparation in this study and relatively homogenous gas environment in the EGA furnace, the current form of the predictive model is most applicable in predicting near-source POA emissions from dry biomass where extensive flaming conditions that produce significant quantities of black or elemental carbon do not occur. The role of fuel moisture in aerosol emission prediction was not within the scope of this work, but should be investigated in future studies. Additionally, the model relies on the presumption of known fuel type and composition, which have been characterized for a broad range of fire fuels (Cai et al., 2017; Carrier et al., 2011; Haghighi Mood et al., 2013; Kan et al., 2016) and geographic vegetation mapping, such as the NASA MODIS vegetation campaign, which has been undertaken at local, national, and global scales (Adam et al., 2010; Xie et al., 2008).

Here, the measured emission factors from cellulose, hemicellulose (xylan), and lignin in 0 and 21 vol% O_2 environments at fuel masses of 0.4, 17.9, and 38.5 mg were used in conjunction with the constituent analysis for pinewood (Table 1) to simulate the emission factors from pinewood at the same conditions and fuel masses. The simulated size-resolved and total number and mass emission factors for the duration of an experiment were determined by

$$EF_{\mathrm{N,sim}} = EF_{N,h}Y_h + EF_{N,c}Y_c + EF_{N,l}Y_l \quad (3)$$

$$EF_{M,sim} = EF_{M,h}Y_h + EF_{M,c}Y_c + EF_{M,l}Y_l \quad (4)$$

where $EF_{N,h}$, $EF_{N,c}$, $EF_{N,l}$, $EF_{M,h}$, $EF_{M,c}$, and $EF_{M,l}$ are the size-resolved or total number and mass emission factors determined for hemicellulose, cellulose, and lignin over the duration of the constituent tests, and Y_h, Y_c, and Y_l are the mass fractions of hemicellulose, cellulose, and lignin, respectively, determined for the pinewood investigated in this study (Table 1).

2.5 Mean Aerosol Diameter

The mean aerodynamic diameters of aerosols formed during pyrolysis or oxidation were determined for the pinewood and biomass constituents as a function of experiment time using real-time measurements of total number and mass aerosol concentrations. These mean diameters allowed for assessment of size differences of aerosols produced in inert and oxidative environments for different fuels, and a better understanding of the discrepancies between the measured and simulated pinewood emission factors. Here, the time-resolved total number concentration ($N_{tot}(t)$) and total mass concentration ($M_{tot}(t)$) of the pinewood and each constituent were determined in 0 and 21 vol% O_2 at a fixed pulverized fuel mass of 17.9 mg and fixed heating rate of 20 °C/min. The mean diameter at each time point was then determined using Equation 5 and results were compared between samples and reaction environments.

$$\mathrm{D_{mean}} = \left(\frac{6M_{tot}(t)}{\pi\rho N_{tot}(t)}\right)^{\frac{1}{3}} \quad (5)$$

2.6 Uncertainty Analysis

Noise in the impactor signal leads to error in measured emissions and must be accounted for. Here, the relative error induced in calculated emissions factors due to signal noise in the cascade

impactor stages was determined following the approach of McLaughlin & Belmont (2021) where stages with signal noise contributing greater than 15% error to the total number and mass emission factor errors were removed for 100% m_{fuel}: $\dot{V}_{dilution}$. The 15% error criterion for 100% m_{fuel}: $\dot{V}_{dilution}$ was selected with the aid of visual inspection of impactor collection plates and raw impactor signals following experimentation. The signal noise contribution to the total emission factor error is determined via the propagation of uncertainty which includes the number concentration uncertainty and the partial derivative of the number emission factor with respect to number concentration for each impactor stage, where the latter includes the ratio of fuel mass to dilution flow rate. The m_{fuel}: $\dot{V}_{dilution}$ was varied between 100, 50, and 25% in this study and, thus, the magnitude of the partial derivative uncertainty term and total error contribution varied by half and a quarter for the 50% and 25% m_{fuel}: $\dot{V}_{dilution}$, respectively, as compared to 100% m_{fuel}: $\dot{V}_{dilution}$. Therefore, stages with signal noise contributing greater than 15%, 7.5% and 3.8% error to the total number and mass emission factor errors were removed from the 100% m_{fuel}: $\dot{V}_{dilution}$, 50% m_{fuel}: $\dot{V}_{dilution,}$ and 25% m_{fuel}: $\dot{V}_{dilution}$ data, respectively, to eliminate data with excessive uncertainty. Comprehensive data sets, which include size-resolved number and mass emission factors for each impactor stage, have been provided in the Supplemental Material, and bins that were excluded are indicated in the comprehensive data sets.

Additionally, noise in the time-resolved number and mass concentration data causes erroneous mean diameter calculations to occur at times in the experiments when the signal-to-noise ratio (SNR) is small, typically in signal regions near the start and end of aerosol formation. The SNR was calculated using the total mass concentration

$$\mathrm{SNR} = \frac{M_{tot,\Delta t}}{U_{M_{tot,\Delta t}}} \tag{6}$$

where $M_{tot,\Delta t}$ is the mean of the total mass concentration measured over a small time period of $\Delta t = 10\ s$, and $U_{M_{tot,\Delta t}}$ is the standard deviation of the total mass concentration over the same small time period. Data points with a SNR less than 5% of the SNR at the time of peak aerosol formation were deemed to have insignificant data signals which did not contribute significantly to the total aerosol formation, and these data points were excluded.

3. Results and Discussion

3.1 Oxidizer Concentration Impact on Pinewood Aerosol Emissions

Size-resolved and total aerosol number emission factors were measured for pinewood pyrolysis and oxidation at a fixed fuel mass of 0.4 mg and at oxygen levels of 0, 1, 2, 5, 14, and 21 vol% O_2 balanced by N_2, and results are shown in Figs. 2 and 3, respectively. Number emissions at each oxygen level were dominated by the particles captured at the smallest aerodynamic bin, having a cut diameter of 0.01 μm, indicating that the majority of the formed aerosols were in the nucleation mode (Rissler et al., 2006). The 0 vol% O_2 environment produced the greatest number of nucleation mode particles among the tested O_2 levels. In addition, the results suggest that more large aerosols in the accumulation mode (Rissler et al., 2006), notably around 0.2 μm, were formed in the two highest oxygen level environments, 14 and 21 vol% O_2, compared to the less oxidative environments. This trend can only be suggested here due to the overlap of 21 vol% O_2 error bars with lower O_2 levels at 0.2 μm, but this trend is investigated more and further supported in Sections 3.2 and 3.3.

The reduction in aerosol number and suggested increased growth with increased O_2 level can be attributed to two dynamics. First, the role of combustion chemistry on aerosol formation must be considered. Consumption of the volatile particle precursor species, which form nucleation mode particles via gas-to-particle conversion, in the oxidative environment reduces aerosol precursor

species below levels present in the inert environment. Additionally, oxidation reactions involving particle precursor species are understood to be influenced by oxygen level and combustion temperature, and these reactions alter the chemistry and volatility of product species (Chu et al., 2019; Glassman, 1979; Kroll & Seinfeld, 2008; Orasche et al., 2013; Reid, Koppmann, et al., 2005; Wey et al., 1984). Low-temperature conversion of biomass will primarily produce holocellulose and lignin pyrolysis products, while high-temperature oxidation will favor the conversion of these species to PAH and oxygenated PAH (Fitzpatrick et al., 2007; Orasche et al., 2013; Reid, Koppmann, et al., 2005), which are soot precursors. Studies of diffusion flames have shown that soot precursor species production and primary soot agglomerate size increase with flame temperature (Chu et al., 2019; Glassman, 1979; Takahashi & Glassman, 1984; Wey et al., 1984), and the adiabatic flame temperature of a diffusion flame in a fuel-rich environment increases with increased oxygen availability (Mitchell et al., 1980; Wey et al., 1985). Further adding to the complex dynamics of combustion chemistry, oxidation reactions that result in the addition of functional groups to precursor species, such as the oxygenation of PAH, can reduce the volatility of those species, although a reduction in carbon chain length can increase volatility (Kroll & Seinfeld, 2008). Taken together, these findings suggest that increased volatile gas combustion temperatures occurred at the higher oxygen levels in this work and resulted in increased formation of high-temperature combustion products which participated in condensation, adsorption, and growth to produce larger aerosols at elevated oxygen levels.

Second, studies have shown that increased BB emission fluxes increase aerosol coagulation and mean aerosol diameter (Sakamoto et al., 2016). Increased fuel consumption rate has been observed at elevated oxygen levels during wood pellet burning, which can be attributed to thermal feedback from volatile gas combustion (Abuelnuor et al., 2014), and this feedback

dynamic was also observed in this study (Section 3.3). Thus, the suggested increased aerosol size produced from pinewood at higher oxygen levels in this study may be attributed to combustion chemistry and increased aerosol coagulation due to an increased fuel consumption rate and correspondingly increased rate of emissions at elevated oxygen levels.

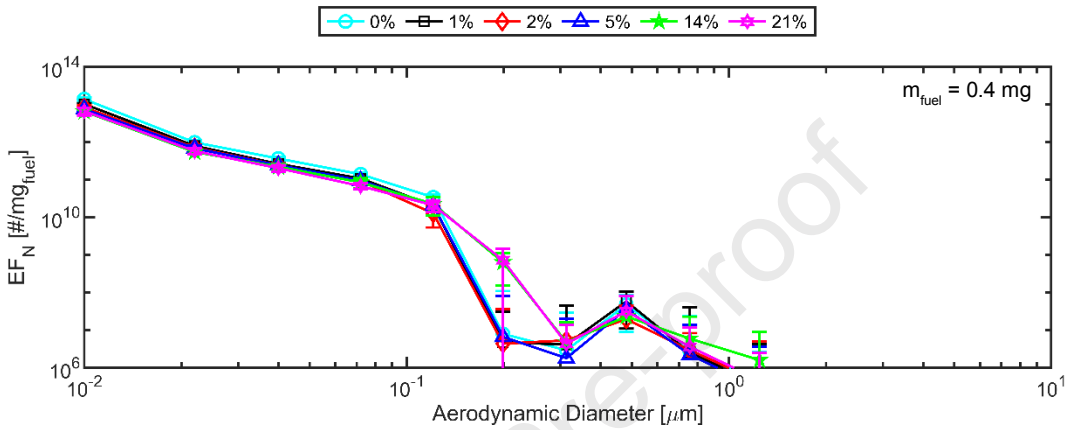

Figure 2. Size-resolved aerosol number emission factors (EF_N) produced from pinewood pyrolysis and oxidation at a fuel mass of 0.4 mg and in 0, 1, 2, 5, 14 and 21 vol% O_2 environments.

The total number emission factor ($EF_{N,tot}$) as a function of reaction environment oxygen level was found by summing the size-resolved number emission factors at each oxygen level and the result is shown in Fig. 3. $EF_{N,tot}$ was also simulated at 0 and 21 vol% O_2 ($EF_{N,tot-sim}$) using measured emissions from the major lignocellulosic biomass constituents at those oxygen levels and applying the summative model, and a comparison with the experimental measurements is also shown in Fig. 3. $EF_{N,tot}$ decreased with increased oxygen level and became constant within uncertainty once the oxygen level reached 14 vol%. $EF_{N,tot}$ decreased from 1.55e13 ± 6.85e11 #/mg_{fuel} to 7.55e12 ± 1.22e12 #/mg_{fuel}, or by 51%, from 0 to 21 vol% O_2. As with the size-resolved number emission factors, this decrease in number is attributed to particle precursor

species that form nucleation mode particles at low oxygen levels being consumed in more highly oxidative environments, as well as increased coagulation and growth related to increased fuel consumption rate and changes to precursor species chemical makeup and volatility due to combustion chemistry (Chu et al., 2019; Fitzpatrick et al., 2007; Glassman, 1979; Hodshire et al., 2019; Kroll & Seinfeld, 2008; Reid, Koppmann, et al., 2005; Sakamoto et al., 2016; Wey et al., 1984). Regarding the model, $EF_{N,tot-sim}$ underpredicted the measured values by 32% and 67% at 0 and 21 vol% O_2, respectively.

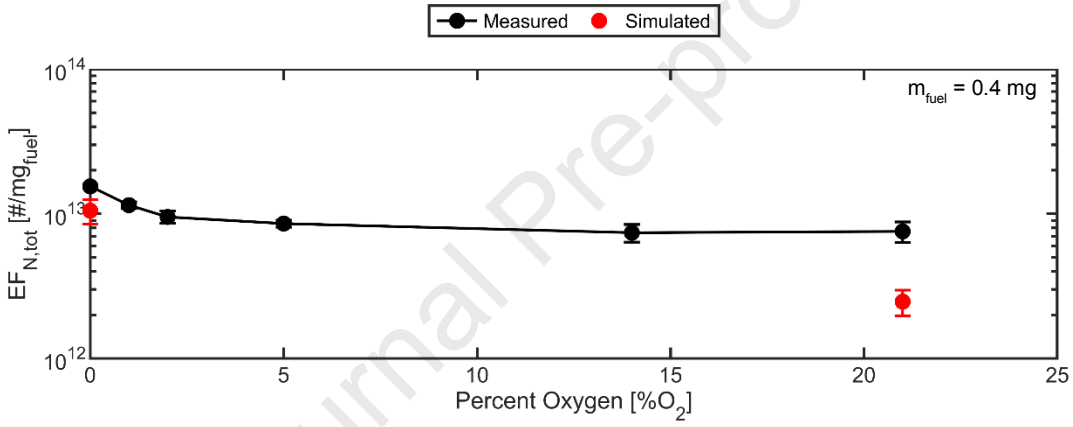

Figure 3. Total aerosol number emission factors ($EF_{N,tot}$) produced from pinewood pyrolysis and oxidation at a fuel mass of 0.4 mg and in 0, 1, 2, 5, 14 and 21 vol% O_2 environments. Black data points are measured values and red data points are simulated values.

Similarly, size-resolved and total mass emission factors were determined for pinewood pyrolysis and oxidation at a fuel mass of 0.4 mg and in 0, 1, 2, 5, 14, and 21 vol% O_2, and results are shown in Figs. 4 and 5, respectively. Impactor detection stages contributing excessive signal uncertainty according to the uncertainty analysis applied in this study were removed from the mass emission factors shown in Figs. 4 and 5, but the comprehensive data set, including the impactor stages that were removed, can be found in the Supplemental Material. Compared to

number emission factors, mass emission factors exhibited much larger uncertainties at larger particle sizes which highlights the cubic effect of diameter on uncertainty propagation when relating number emissions to mass emissions.

Figure 4 shows the size-resolved mass emission factors (EF_M) for pinewood at a fuel mass of 0.4 mg and each tested oxygen level. Results again suggest that, similar to EF_N, larger accumulation mode particles around 0.2 μm in diameter were formed at higher oxygen levels of 14 and 21 vol% O_2 compared to lower oxygen levels, and the increased size of aerosols in higher oxygen level environments is confirmed in Section 3.3. This may again be attributed to the complex influences of combustion chemistry on aerosol precursor species and also increased aerosol coagulation arising from increased fuel consumption rates due to thermal feedback from volatile gas combustion occurring near the solid fuel in higher oxygen level environments (Chu et al., 2019; Fitzpatrick et al., 2007; Glassman, 1979; Hodshire et al., 2019; Kroll & Seinfeld, 2008; Orasche et al., 2013; Reid, Koppmann, et al., 2005; Sakamoto et al., 2016; Wey et al., 1984). The peak EF_M occurred in an aerodynamic diameter bin size of 0.07 μm for 1 and 2 vol% O_2 and a bin size of 0.12 μm for 0, 5, 14 and 21 vol% O_2. The size distributions of EF_M are distinctly different from EF_N in that the nucleation mode particles do not dominate EF_M. Rather, the larger aerosols near 0.1 μm are observed to be the most prominent in EF_M. This difference between EF_N and EF_M was expected because $EF_{M,i}$ is proportional to the product of $EF_{N,i}$ and the cube of D_i.

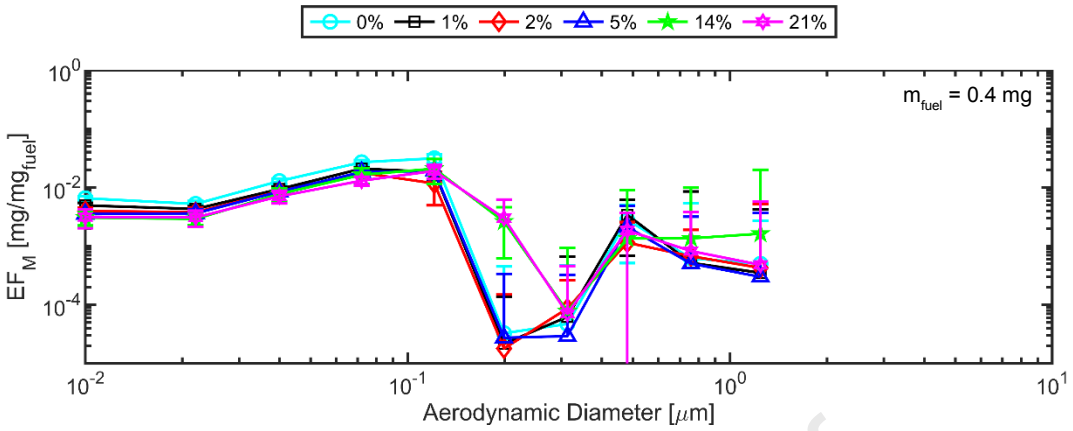

Figure 4. Size-resolved aerosol mass emission factors (EF_M) produced from pinewood pyrolysis and oxidation at a fuel mass of 0.4 mg and in 0, 1, 2, 5, 14, and 21 vol% O_2.

The total mass emission factors ($EF_{M,tot}$) produced from pinewood pyrolysis and oxidation were determined by summing the size-resolved mass emission factors at each oxygen level. The results are shown in Fig. 5 alongside the simulated results, $EF_{M,tot-sim}$, which were determined using measured emissions from the major lignocellulosic biomass constituents and the summative model. Similar to $EF_{N,tot}$, $EF_{M,tot}$ decreased initially with increased oxygen level and then became constant within uncertainty at an oxygen level of 5 vol% and higher. $EF_{M,tot}$ decreased from 0.0871 ± 0.0071 mg/mg_{fuel} to 0.0544 ± 0.0049 mg/mg_{fuel}, or by 37%, from 0 to 21 vol% O_2, which is a smaller decrease compared to the decrease in $EF_{N,tot}$. This relatively small change was attributed to competing influences of decreased number of smaller particles due to consumption of precursor gases in an oxidative environment – decreasing $EF_{M,tot}$ – and increased aerosol size due to combustion chemistry as well as increased fuel consumption rate and coagulation due to volatile combustion thermal feedback – increasing $EF_{M,tot}$ (Chu et al., 2019; Fitzpatrick et al., 2007; Glassman, 1979; Hodshire et al., 2019; Kroll & Seinfeld, 2008; Orasche et al., 2013; Reid, Koppmann, et al., 2005; Sakamoto et al., 2016; Wey et al., 1984).

$EF_{M,tot-sim}$ agreed well with the measured value at 21 vol% O_2, within 15%, while $EF_{M,tot-sim}$ less successfully captured the measured value in the 0 vol% O_2 environment, within 376%. The agreement and disagreement between the model and experiments are discussed further in Sections 3.2 and 3.3.

$EF_{M,tot}$ measured in this study for pyrolysis of pinewood in 0 vol% O_2 (87.1 ± 7.1 g/kg$_{fuel}$) was larger than mass emission factors typically reported for pinewood burning, such as those by Hays et al. (2002) for the Pinaceae family (11.2-33.5 g/kg$_{fuel}$), those by Vose et al. (1996) for pinewood forest wildfire and logging slash burning (7.5-62.5 g/kg$_{fuel}$), and those by Grandesso et al. (2011) for loblolly pine burning (7-77 g/kg$_{fuel}$). Such discrepancies are to be expected in the absence of volatile particle precursor species consumption by oxidation before particle formation in the pyrolysis experiments of this study as compared to the burning scenarios in the aforementioned studies, all of which included oxidation. A more direct comparison with the $EF_{M,tot}$ of the pinewood in the oxidative conditions of 1-21 vol% O_2 in the present study (48.2 ± 7.3 to 54.4 ± 4.9 g/kg$_{fuel}$), shows that the results of this study fall within the upper limit of the range of mass emission factors reported for pinewood burning by Vose et al. (1996) and Grandesso et al. (2011).

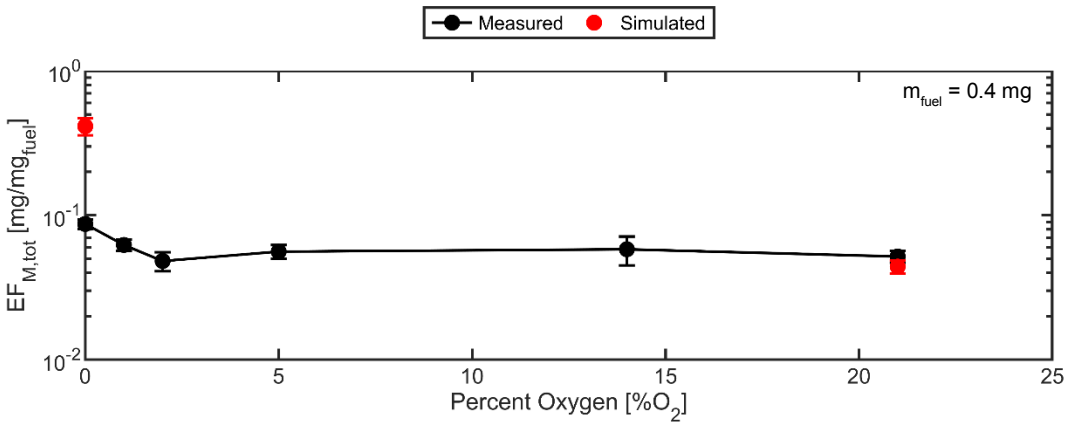

Figure 5. Total aerosol mass emission factors ($EF_{M,tot}$) produced from pinewood pyrolysis and oxidation at a fuel mass of 0.4 mg and in 0, 1, 2, 5, 14, and 21 vol% O_2. Black data points are measured values and red data points are simulated values.

In order to better understand the impacts of reaction environment oxygen level on aerosol number and mass emissions from pinewood pyrolysis and combustion, temporally resolved total aerosol number concentration was investigated at each oxygen level. The total aerosol number concentration, calculated as the sum of number concentrations at each impactor stage, formed from pinewood during pyrolysis and oxidation was determined as a function of test time and reaction environment temperature at a fuel mass of 0.4 mg and in 0, 1, 2, 5, 14, and 21 vol% O_2 environments, and results are shown in Fig. 6. The test results are plotted between test times of 1100 s and 2300 s to highlight details in aerosol formation at each oxygen level, as the majority of aerosols formed during this time period. Onset and early aerosol formation are similar for all oxygen levels in the pre-ignition regime up to approximately 1550 s, corresponding to an environment temperature of 325 °C, and the maximum aerosol formation was of similar magnitude across the different tested oxygen levels. The maximum aerosol formation, however, occurred at earlier times, corresponding to lower reaction environment temperatures, as the oxygen level increased. Additionally, the duration of the major aerosol formation event was observed to decrease with increased oxygen level and is indicated by the decreased time over which a significant number concentration was measured. This may be attributable to oxidation of volatile particle precursor species and resulting thermal feedback which increased the fuel consumption rate of the pinewood at elevated oxygen levels (shown in Section 3.3). The environment temperatures at peak derivative mass loss for oxygen levels of 0, 1, 2, 5, 14, and 21

vol% O_2 were determined to be 385, 380, 378, 368, 361, and 358 °C, respectively. The decrease in these temperatures indicates earlier ignition of gas-phase volatiles with increase in O_2 level.

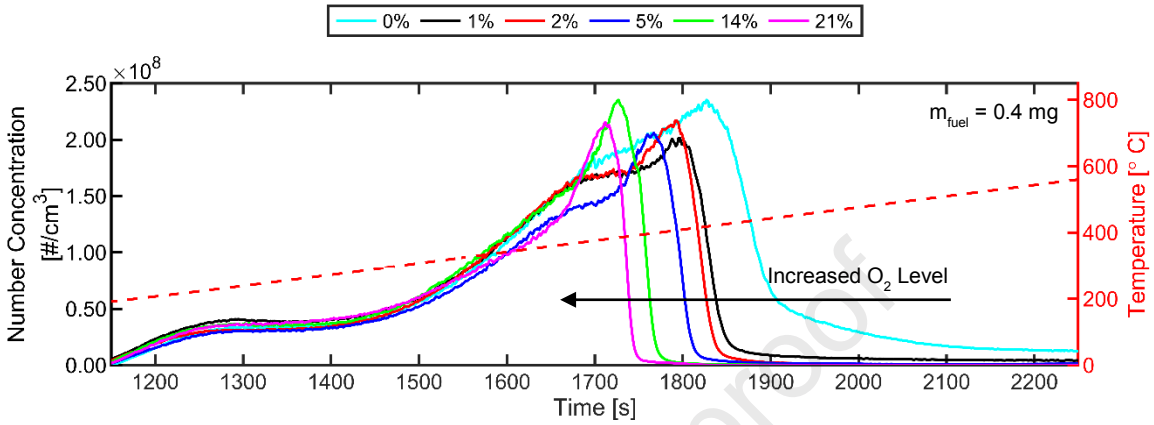

Figure 6. Total aerosol number concentration as a function of test time, produced from pinewood pyrolysis and oxidation at a fuel mass of 0.4 mg and in 0, 1, 2, 5, 14, and 21 vol% O_2. Reaction environment temperature is also shown.

3.2 Fuel Mass Impact on Pinewood and Constituent Aerosol Emissions

$EF_{N,tot}$ was measured for pinewood in 0 and 21 vol% O_2 environments at fuel masses of 0.4, 1.0, 1.8, 9.0, 17.9, and 35.8 mg. Results are shown in Fig. 7, and Table 3 is provided for assistance in interpreting the legend. The measured $EF_{N,tot}$ for pinewood decreased with increased fuel mass, from 1.55e13 ± 6.85e13 #/mg_{fuel} to 1.13e12 ± 3.84e10 #/mg_{fuel} and 7.55e12 ± 1.22e12 #/mg_{fuel} to 6.43e11 ± 3.85e10 #/mg_{fuel}, or by 93% and 91%, when fuel mass was increased from 0.4 mg to 35.8 mg for the 0 and 21 vol% O_2 environments, respectively. Comparing the $EF_{N,tot}$ produced in the 0 and 21 vol% O_2 environments at the same fuel masses, $EF_{N,tot}$ were an average of 46% greater in the 0 vol% O_2 environment than in the 21 vol% O_2 environment across all of the investigated fuel masses. This environment dependence was again attributed to consumption of

volatile particle precursor species by combustion in the 21 vol% O_2 environment, compared to no oxidation occurring in the 0 vol% O_2 environment, as well as chemical alteration of particle precursor species and coagulation and growth as discussed in Section 3.1 (Chu et al., 2019; Fitzpatrick et al., 2007; Glassman, 1979; Hodshire et al., 2019; Kroll & Seinfeld, 2008; Orasche et al., 2013; Reid, Koppmann, et al., 2005; Sakamoto et al., 2016; Wey et al., 1984).

The decrease in $EF_{N,tot}$ with increased fuel mass further supports the suggestion that coagulation plays a role in aerosol numbers measured in these experiments, as larger fuel masses will generate greater emissions fluxes under comparable pyrolysis or oxidation conditions, as shown for an oxidative environment in Fig. 9b. The influence of fuel consumption rate was investigated by varying the fuel heating rate from 20 °C/min to 10 °C/min and 50 °C/min in 0 vol% O_2 at a pulverized fuel mass of 17.9 mg and at 50% m_{fuel}: $\dot{V}_{dilution}$. The higher heating rate of 50 °C/min resulted in the highest peak fuel mass loss rate (39.0 mass% /min) compared the 20 °C/min (18.1 mass%/min) and 10 °C/min (9.3 mass%/min) heating rates, and the resultant $EF_{N,tot}$ (Fig. 7) decreased by 50% and 48% when increasing the heating rate from 10 °C/min to 20 °C/min and 20 °C/min to 50 °C/min, respectively. While the heating rate test was performed in an inert environment to eliminate thermal feedback from combustion and thereby better control the heating rate, the reduction of $EF_{N,tot}$ that was measured in an oxidative environment can likewise be understood as resulting from increased heating rate due to volatile combustion thermal feedback and resultant increased emission mass flux and increased coagulation, in addition to consumption and chemical alteration of particle precursor species in an oxidative environment (Chu et al., 2019; Fitzpatrick et al., 2007; Glassman, 1979; Hodshire et al., 2019; Kroll & Seinfeld, 2008; Orasche et al., 2013; Reid, Koppmann, et al., 2005; Sakamoto et al., 2016; Wey et al., 1984).

The first of several checks for other influences on $EF_{N,tot}$ examined the impact of m_{fuel}: $\dot{V}_{dilution}$ on aerosol emissions in a 21 vol% O_2 environment, and a maximum difference of 17% was observed between 100%, 50%, and 25% m_{fuel}: $\dot{V}_{dilution}$. Next, the influences of residence time and experimental sampling apparatus size on $EF_{N,tot}$ were investigated at a fuel mass of 1.8 mg at 100% m_{fuel}: $\dot{V}_{dilution}$ in a 21 vol% O_2 environment. $EF_{N,tot}$ at a residence time of 2.5 s agreed with that of a 2.3 s residence time within 51%. $EF_{N,tot}$ produced at a residence time of 2.5 s in the large sampling apparatus agreed with that of the small sampling apparatus, in which a 2.5 s residence time was also achieved via added tubing length, within 27%.

$EF_{N,tot}$ was simulated for pinewood ($EF_{N,tot-sim}$) and compared to the measured pinewood $EF_{N,tot}$ using the developed summative model at fuel masses of 0.4, 17.9 and 35.8 mg. Model results followed the trends and matched the magnitudes of the measured pinewood $EF_{N,tot}$ in both the 0 and 21 vol% O_2 environments at all fuel masses. $EF_{N,tot-sim}$ in 0 and 21 vol% O_2 underpredicted the measured values within an average of 38% and 56%, respectively, across the 0.4, 17.9, and 35.8 mg fuel masses.

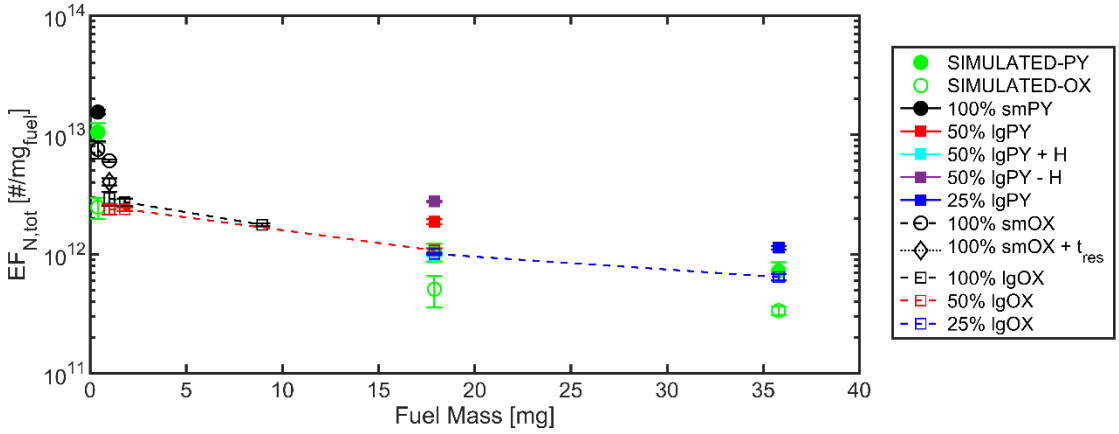

Figure 7. Total aerosol number emission factors ($EF_{N,tot}$) as a function of fuel mass, produced from pinewood and simulated pinewood pyrolysis and oxidation at 0 vol% (PY) and 21 vol%

(OX) O_2. Dashed lines connect multiple data points taken at similar experimental conditions. Table 3 provides legend details, and results in this plot are tabulated in the Supplemental Material because data markers overlap one another and may be difficult to see in the plot.

Similarly, $EF_{M,tot}$ was measured for the pinewood in 0 and 21 vol% O_2 at fuel masses of 0.4, 1.0, 1.8, 9.0 17.9, and 35.8 mg, and results are shown in Fig. 8a. As previously noted, impactor stages contributing signal noise exceeding the established criteria were removed from the data, but the comprehensive data tables including and highlighting removed stages are provided in the Supplemental Material. The measured $EF_{M,tot}$ of pinewood, unlike $EF_{N,tot}$, were observed to slightly decrease and increase in 0 and 21 vol% O_2 environments, respectively, across all investigated fuel masses. $EF_{M,tot}$ were found to be 0.0870 ± 0.0071 mg/mg$_{fuel}$ and 0.0544 ± 0.0049 mg/mg$_{fuel}$ at a fuel mass of 0.4 mg, and 0.0739 ± 0.0032 mg/mg$_{fuel}$ and 0.0750 ± 0.0048 mg/mg$_{fuel}$ at a fuel mass of 35.8 mg, in 0 and 21 vol% O_2 environments, respectively, resulting in a decrease of 15% and an increase of 38% from 0.4 mg to 35.8 mg in the 0 and 21 vol% O_2 environments, respectively. Although the fuel masses investigated in this study were significantly smaller than the fuel masses that burn in wildland fires, the relatively small change in $EF_{M,tot}$ for pinewood in both reaction environments across the three orders of magnitude range of tested fuel masses is supported by previous works, which found that total particulate mass emission factors produced from 275-1100 g of corn stover burning in a cookstove (Shen et al., 2013) and 1-10 kg of loblolly pine burning in a closed chamber (Grandesso et al., 2011) were independent of fuel mass load.

When averaged over all tested fuel masses, $EF_{M,tot}$ produced in the 0 and 21 vol% O_2 environments were within 10% of each other, and the average $EF_{M,tot}$ across all fuel masses in

the 0 and 21 vol% O_2 environments were 0.0755 ± 0.0042 mg/mg_{fuel} and 0.0672 ± 0.0078 mg/mg_{fuel}, respectively. While 0 vol% O_2 emissions slightly exceeded those of 21 vol% O_2 on average, $EF_{M,tot}$ in 21 vol% O_2 slightly exceeded that of 0 vol% O_2 at the largest fuel mass of 35.8 mg. This result further suggests that $EF_{M,tot}$ is influenced by aerosol precursor species consumption via oxidation, growth due to oxidative reactions that alter the chemical makeup and volatility of emissions, and growth due to increased fuel consumption rates and coagulation from volatile combustion thermal feedback at elevated oxygen levels (Chu et al., 2019; Fitzpatrick et al., 2007; Glassman, 1979; Hodshire et al., 2019; Kroll & Seinfeld, 2008; Orasche et al., 2013; Reid, Koppmann, et al., 2005; Sakamoto et al., 2016; Wey et al., 1984). Overall, as was discussed in Section 3.1 for the 0.4 mg fuel mass results, the average 0 vol% O_2 $EF_{M,tot}$ exceeded mass emission factors typically reported for pinewood burning, while the average 21 vol% O_2 $EF_{M,tot}$ is within the reported mass emission factor range for pinewood fires (Grandesso et al., 2011; Hays et al., 2002; Vose et al., 1996).

Increases in heating rate from 10 °C/min to 20 °C/min and 20 °C/min to 50 °C/min were found to increase and decrease $EF_{M,tot}$ by 3% and 0.4%, respectively, in 0 vol% O_2 at a fuel mass of 17.9 mg and 50% m_{fuel}: $\dot{V}_{dilution}$, contrary to the influence on $EF_{N,tot}$. Size-resolved EF_M profiles (Fig. 8b) showed that increased heating rate reduced the number of ultrafine aerosols and increased larger accumulation mode aerosols, resulting in a decrease of $EF_{N,tot}$ and statistical conservation of $EF_{M,tot}$. It is noted that a statistically significant increase of aerosol size with increased heating rate is observed in the 0.48 μm bin diameter, whereas the data at larger bin diameters overlap within uncertainty. This result shows that aerosol coagulation occurred during the tests conducted in this work and increased with increased fuel consumption rate. Furthermore, this result also supports the suggested findings in Section 3.1 that increased aerosol

sizes were observed at elevated oxygen levels, which can now be better understood as resulting from influences of increased fuel consumption rates and particle coagulation, as well as combustion chemistry (Chu et al., 2019; Fitzpatrick et al., 2007; Glassman, 1979; Hodshire et al., 2019; Kroll & Seinfeld, 2008; Orasche et al., 2013; Reid, Koppmann, et al., 2005; Sakamoto et al., 2016; Wey et al., 1984).

Similar sensitivity tests to those performed on $EF_{N,tot}$ were performed for $EF_{M,tot}$ as well. A maximum difference of 10% between the pinewood $EF_{M,tot}$ at 100%, 50%, and 25% m_{fuel}: $\dot{V}_{dilution}$ was measured across all fuel masses in the 21 vol% O_2 environment. The influence of residence time and experimental sampling apparatus size on mass emissions was investigated and the $EF_{M,tot}$ at 2.5 s agreed with that of 2.3 s within 22%, while $EF_{M,tot}$ at a residence time of 2.5 s from the large sampling apparatus agreed with that of the small sampling apparatus with added residence time within 9%.

$EF_{M,tot}$ was simulated for pinewood ($EF_{M,tot-sim}$) and compared to the measured pinewood $EF_{M,tot}$ using the summative model at fuel masses of 0.4, 17.9 and 35.8 mg. Simulated values agreed well with the trend and magnitude of the measured values in the 21 vol% O_2 environment as a function of fuel mass. $EF_{M,tot-sim}$ at 21 vol% O_2 overpredicted the measured values at 17.9 mg and 35.8 mg and underpredicted the measured value at 0.4 mg and, overall, $EF_{M,tot-sim}$ agreed with the measured values within an average of 56% across the 0.4, 17.9, and 35.8 mg fuel mass comparisons. However, the model less successfully captured the magnitude of the measured pinewood $EF_{M,tot}$ in the 0 vol% O_2 environment. $EF_{M,tot-sim}$ at 0 vol% O_2 overpredicted the measured values at each fuel mass within an average of 330% across comparable fuel masses.

Additionally, the summative model was tested against an experimentally measured total aerosol mass emission factor for miscanthus burning in air in a TGA, which was measured to be 55 mg/g_{fuel} by Dorge et al. (2011). Lignocellulosic constituent contents for *Miscanthus* × *giganteus* reported by Lee et al. (2015) were 34% cellulose, 32% hemicellulose, and 26% lignin by mass. Using this composition and the average constituent emissions measured in the present study across each of the tested fuel masses in the 21 vol% O_2 environment, $EF_{M,tot-sim}$ of miscanthus was found to be within 87% of the value measured by Dorge et al. in an oxidative environment. Similar to pine, $EF_{M,tot}$ was overpredicted by the model for miscanthus.

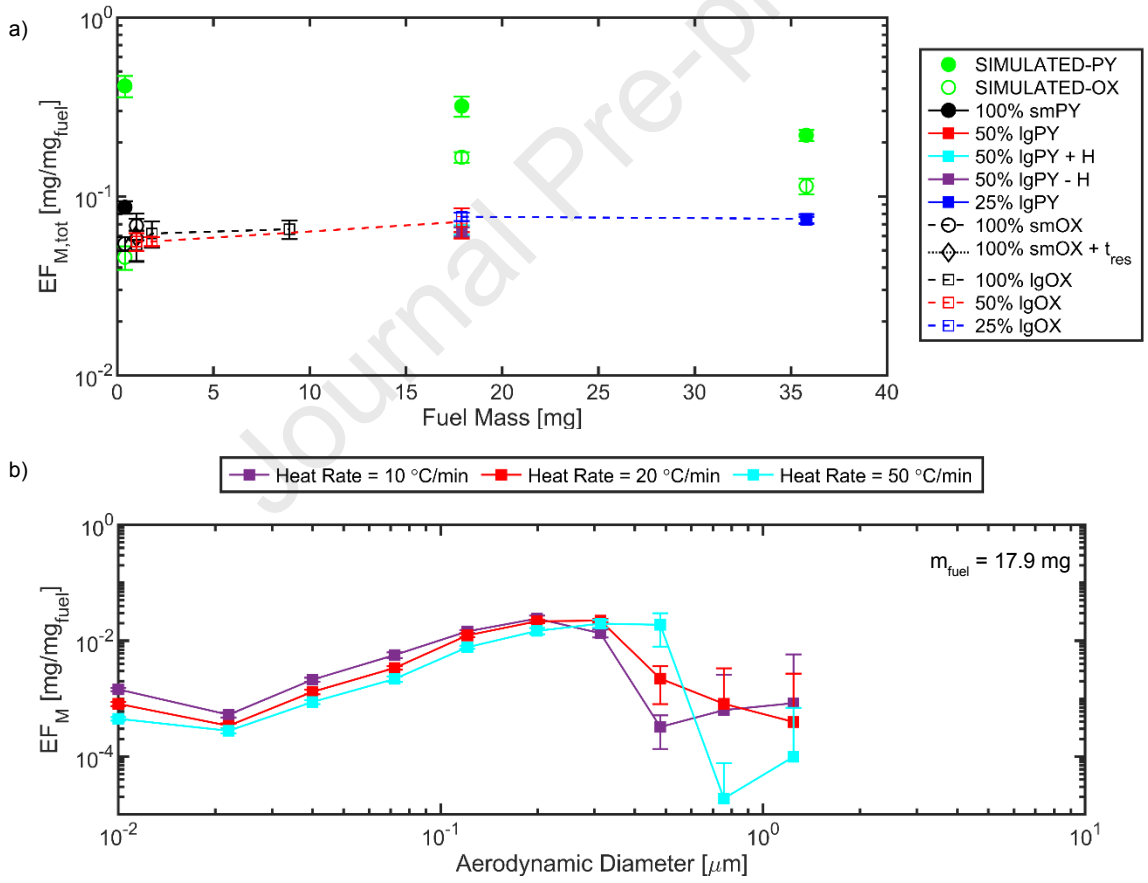

Figure 8. a) Total aerosol mass emission factors ($EF_{M,tot}$) as a function of fuel mass, produced from pinewood and simulated pinewood pyrolysis and combustion at 0 vol% (PY) and 21 vol%

(OX) O_2 and b) size-resolved mass emission factors (EF_M) resulting from the varied heating rate tests of pinewood in 0 vol% (PY) O_2 at a fuel mass of 17.9 mg and 50% m_{fuel}: $\dot{V}_{dilution}$. Dashed lines connect multiple data points taken at similar experimental conditions. Table 3 provides legend details, and results in this plot are tabulated in the Supplemental Material because some data markers overlap one another and may be difficult to see in the plot.

In contrast to $EF_{N,tot}$, which decreased 93% and 91% in the 0 and 21 vol% O_2 environments, respectively, as fuel mass increased, $EF_{M,tot}$ decreased 15% and increased 38% in the 0 and 21 vol% O_2 environments, respectively, as fuel mass increased. These trends can be better understood by examining the size-resolved mass emission factors (Fig. 9a) and fuel mass consumption rate profiles (Fig. 9b) of pinewood at fuel masses of 0.4, 1.8, and 35.8 mg and at 100% m_{fuel}: $\dot{V}_{dilution}$, 50% m_{fuel}: $\dot{V}_{dilution}$, and 25% m_{fuel}: $\dot{V}_{dilution}$, respectively, in a 21 vol% O_2 environment. Additionally, emission factor results for pinewood at a fuel mass of 1.8 mg and 100% m_{fuel}: $\dot{V}_{dilution}$ were plotted for comparison to the 50% m_{fuel}: $\dot{V}_{dilution}$ at the same fuel mass to better understand the influence of m_{fuel}: $\dot{V}_{dilution}$ on aerosol emission size distributions (Fig. 9a). The numbers of small particles – nucleation mode and Aitken mode particles – decreased and the numbers of larger particles – accumulation mode and coarse particles – increased with increased fuel mass. The shift of the aerosol size distributions from small particles to large particles with increased fuel mass, also observed in a study of corn straw burning by Shen et al. (2013), was responsible for the decreasing and slightly differing trends of $EF_{N,tot}$ and $EF_{M,tot}$, respectively, in 0 and 21 vol% O_2 as fuel mass increased. Notably, the same trends for small and large particles were observed with increased heating rate (Fig. 8b). Taken together, these results may be attributable to the increased rate of fuel consumption with increased fuel mass (Fig. 9b) and/or thermal feedback by oxidation. Furthermore, while an increased fuel consumption rate in 0 vol%

O_2 statistically conserved $EF_{M,tot}$ during the varied heating rate tests, the 38% increase of $EF_{M,tot}$ with increased fuel mass in 21 vol% O_2 further suggests that combustion chemistry has a significant role in aerosol formation, such as via the formation of PAH and other high-temperature oxidation products that have reduced volatility and form nucleation sites for adsorption and aerosol growth (Fitzpatrick et al., 2007; Glassman, 1979; Kroll & Seinfeld, 2008; Orasche et al., 2013; Reid, Koppmann, et al., 2005; Takahashi & Glassman, 1984). The results here, with support from the cited literature, suggest that the combustion temperature increased with fuel consumption rate in the oxidative environment and subsequently increased high-temperature combustion product production and $EF_{M,tot}$ in 21 vol% O_2 with increased fuel mass. Regarding m_{fuel}: $\dot{V}_{dilution}$, EF_M for pinewood at 1.8 mg and 50% m_{fuel}: $\dot{V}_{dilution}$ agreed with that of pinewood at 1.8 mg and 100% m_{fuel}: $\dot{V}_{dilution}$ within an average of 51% across all aerodynamic diameter size bins, suggesting that m_{fuel}: $\dot{V}_{dilution}$ as investigated in this work has a small influence on the size and number of aerosol emissions.

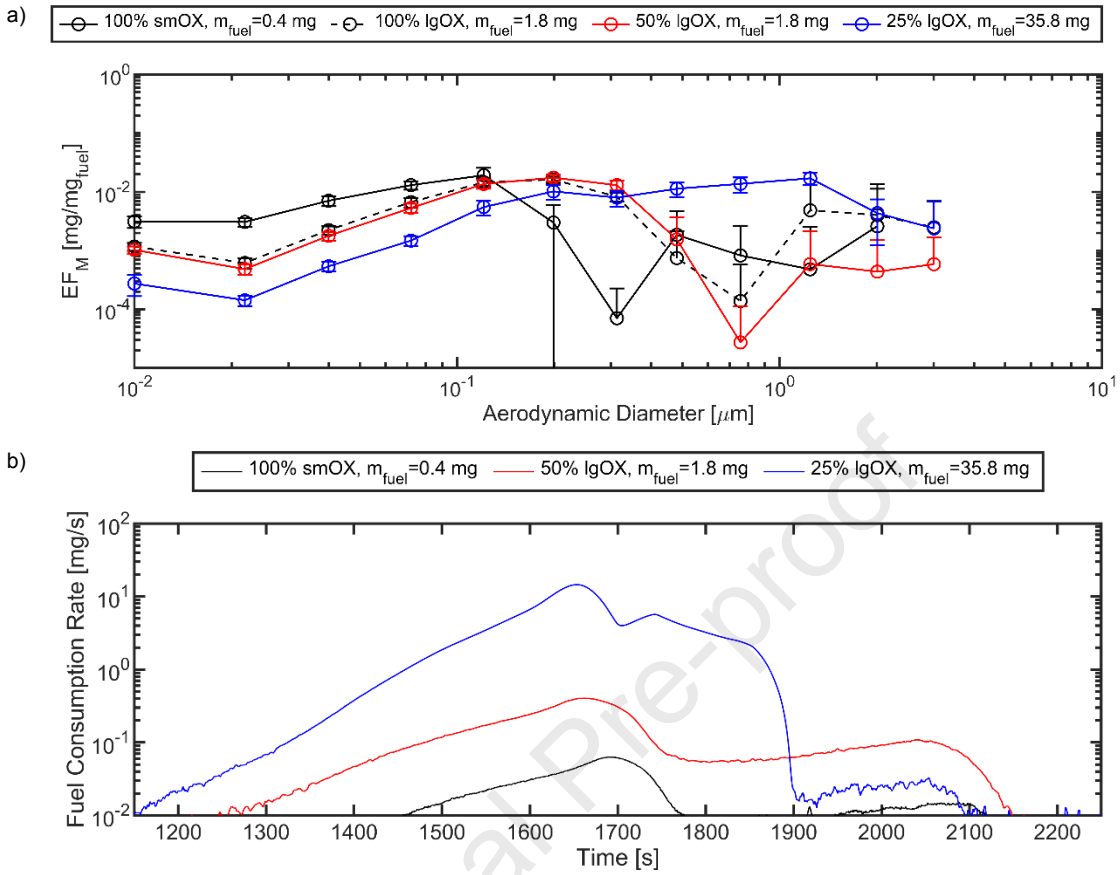

Figure 9. a) Size-resolved aerosol mass emission factors (EF_M) and b) fuel consumption rates as a function of test time, produced from pinewood combustion in 21 vol% (OX) O_2 for fuel masses of 0.4 mg, 1.8 mg, and 35.8 mg.

Considering that m_{fuel}: $\dot{V}_{dilution}$, sampling apparatus size, and residence time were all shown to minimally influence aerosol emissions in Figs. 7, 8, and 9, the results indicate that the formation, coagulation, and growth of aerosols occur rapidly upstream of the dilution point where the tested m_{fuel}: $\dot{V}_{dilution}$ are achieved. While m_{fuel}: $\dot{V}_{dilution}$ was carefully controlled in this study, this control occurred about 1.5 s downstream of the fuel sample due to the low flow rate exiting the TGA. The TGA flow rate was fixed at 0.1 SLPM due to limitations of the equipment, resulting in increased aerosol precursor species concentrations in the gas stream prior to dilution as fuel mass

increased. Increased precursor species concentrations are understood to lead to increased gas-to-particle conversion (May et al., 2013), resulting in an increased particle number concentration initially emitted from the burning event which is understood to increase aerosol coagulation and mean aerosol diameter (Sakamoto et al., 2016). Greater numbers of precursor species are expected to be present during pyrolysis compared to combustion due to the consumption of precursor species in the oxidative environment. There is also a lack of combustion chemistry influences, and slower fuel consumption rates are expected during pyrolysis of pinewood as compared to combustion. The net result of these competing effects is reflected in the near-constant $EF_{M,tot}$ (15% decrease) and increase (38%) of $EF_{M,tot}$ with increased fuel mass in 0 and 21 vol% O_2, respectively. Ultimately, aerosol emissions were insensitive to m_{fuel}: $\dot{V}_{dilution}$ and its associated parameters of sampling apparatus size and residence time, and results indicate that the formation and transition of nucleation mode particles to larger accumulation mode particles occurs rapidly within the approximately 1.5 s residence time of the TGA and sample line prior to dilution.

3.3 Biomass and Constituent Mean Aerosol Diameter During Pyrolysis and Oxidation

The mean aerodynamic aerosol diameter was determined for a fuel mass of 17.9 mg at a 50% m_{fuel}: $\dot{V}_{dilution}$ as a function of test time for the pinewood and the major lignocellulosic biomass constituents of hemicellulose (xylan), cellulose, and lignin to better understand the success and failure of the summative model in prediction of aerosol number and mass emission factors in 0 and 21 vol% O_2 environments (Fig. 10). Figure 10a shows that a greater maximum mean aerosol diameter of 0.123 μm was reached for pinewood, and at an earlier test time corresponding to a lower reaction environment temperature of 335 °C, in 21 vol% O_2 compared to the maximum mean aerosol diameter of 0.061 μm reached at a reaction environment temperature of 383 °C in 0

vol% O_2. The finding that larger aerosols were formed from pinewood at higher oxygen concentrations further suggests that combustion chemistry influences aerosol formation, and also supports the suggested finding in Section 3.1 that larger aerosols formed from pinewood in 21 vol% O_2 compared to 0 vol% O_2. Figure 10a also shows the fuel mass loss profiles of pinewood in 0 and 21 vol% O_2 environments. The pinewood lost a majority of its mass in the 21 vol% O_2 environment at an earlier test time, lower reaction environment temperature, and faster rate compared to the 0 vol% O_2 environment. The result is indicative of ignition of the volatiles and thermal feedback to the biomass sample in the 21 vol% O_2 environment, and supports previous claims that the pinewood fuel consumption rate is increased in oxidative environments compared to inert environments. These results also support the results shown in Fig. 6, where the maximum aerosol formation event occurred at earlier test times and lower reaction environment temperatures in highly oxidative environments, now understood to coincide with the major fuel mass loss event.

Figure 10b shows the mean aerodynamic diameter for hemicellulose (xylan). The maximum mean aerosol diameter of approximately 0.032 μm occurred at a reaction environment temperature of 263 °C and did not significantly differ between the 0 and 21 vol% O_2 environments. Likewise, the total mass loss and fuel consumption rate over the period of maximum aerosol diameter formation was similar between the pyrolysis and oxidation tests due to the majority of mass loss occurring from xylan below its ignition temperature. Because hemicellulose produced an insignificant number of particles (see Supplemental Material) no hypothesis regarding the relationship between aerosol growth and oxidation level was made for hemicellulose.

Figure 10c shows the mean aerodynamic diameters for cellulose. The maximum mean aerosol diameters of cellulose were 0.521 μm and 0.507 μm at corresponding reaction environment temperatures of 350 °C and 337 °C in the 0 and 21 vol% O_2 environments, respectively. A significant change in aerosol diameter was not observed, nor did the mass loss profiles and fuel consumption rates differ significantly between the reaction environments. Similarities in aerosol diameters between the two environments may be attributable to similar fuel consumption rates and mass loss occurring prior to ignition, as was the case for xylan, as well as similarities in products of cellulose pyrolysis and oxidation at low temperatures before volatile ignition (Fitzpatrick et al., 2007). Additionally, the cellulose result shows a significant second peak mean aerosol diameter near 2700 s in the inert and oxidative environments. It should be noted that significant aerosol production is not occurring at this test time, and the increase in aerosol diameter may be due to further pyrolysis and oxidation of the cellulose at temperatures near 750 °C, releasing additional particle precursor species.

In contrast to the negligible differences observed between reaction environments for hemicellulose and cellulose, the mean aerodynamic diameter of lignin (Fig. 10d) reached a greater maximum of 0.147 μm in 0 vol% O_2 compared to a maximum of 0.031 μm in 21 vol% O_2. These maximum diameters occurred at reaction environment temperatures of 403 °C and 400 °C, respectively. The increased growth in the inert environment is supported by the mass loss rate of the lignin in the inert environment exceeding that of the oxidative environment until about 550 °C when ignition occurs, beyond the peak aerosol formation temperature. These results are consistent with other results of this work indicating that increased fuel consumption rate leads to increased aerosol size. Similar to cellulose, lignin produced a notable second peak in mean aerosol diameter near 3100 s in the inert and oxidative environments. The second peak diameter

of lignin also occurred at a test time where few aerosols were being formed, and the trend was again attributed to further pyrolysis and oxidation of the lignin at elevated reaction environment temperatures in inert and oxidative environments, respectively.

The relative success and failure of the summative model in predicting total mass emission factors in the oxidative and inert environments, respectively, may be due to an overprediction of large aerosols produced during the peak pyrolysis mass loss event based on the lignin emission factor input to the model in the 0 vol% O_2 environment. The results suggest that the representative lignin sample chosen for this work may not accurately capture the pyrolysis behavior of the lignin in the actual pinewood, as lignin decomposition products are expected to be similar in inert and oxidative environments at lower temperatures prior to ignition (Fitzpatrick et al., 2007). If true, agreement between the model and measurements could be improved by a more representative lignin sample which produces fewer large aerosol particles at the peak aerosol formation event during pyrolysis. It is recognized that lignocellulosic biomass constituents in the native biomass have slightly different structures than those of the representative constituents used in this work (Qu et al., 2011), and lignin pyrolysis products are understood to vary significantly amongst species and biomass families such as softwoods, grasses, and hardwoods (Buranov & Mazza, 2008). While the lignin chosen in this work is derived from softwood, including pine, it is likely that the processing required for its production altered its chemistry and structure.

It is further concluded from the comparison of the model, experiments, and mean aerosol aerodynamic diameter results that the cellulose content of the lignocellulosic biomass is a primary producer of large, accumulation mode aerosols during biomass burning. This conclusion is supported by a previous study which showed no evidence that lignin pyrolysis products

contribute to the growth of aerosols (Mochida & Kawamura, 2004). Furthermore, hemicellulose was found to contribute little to the total number and mass emission factors during oxidation and pyrolysis in this work.

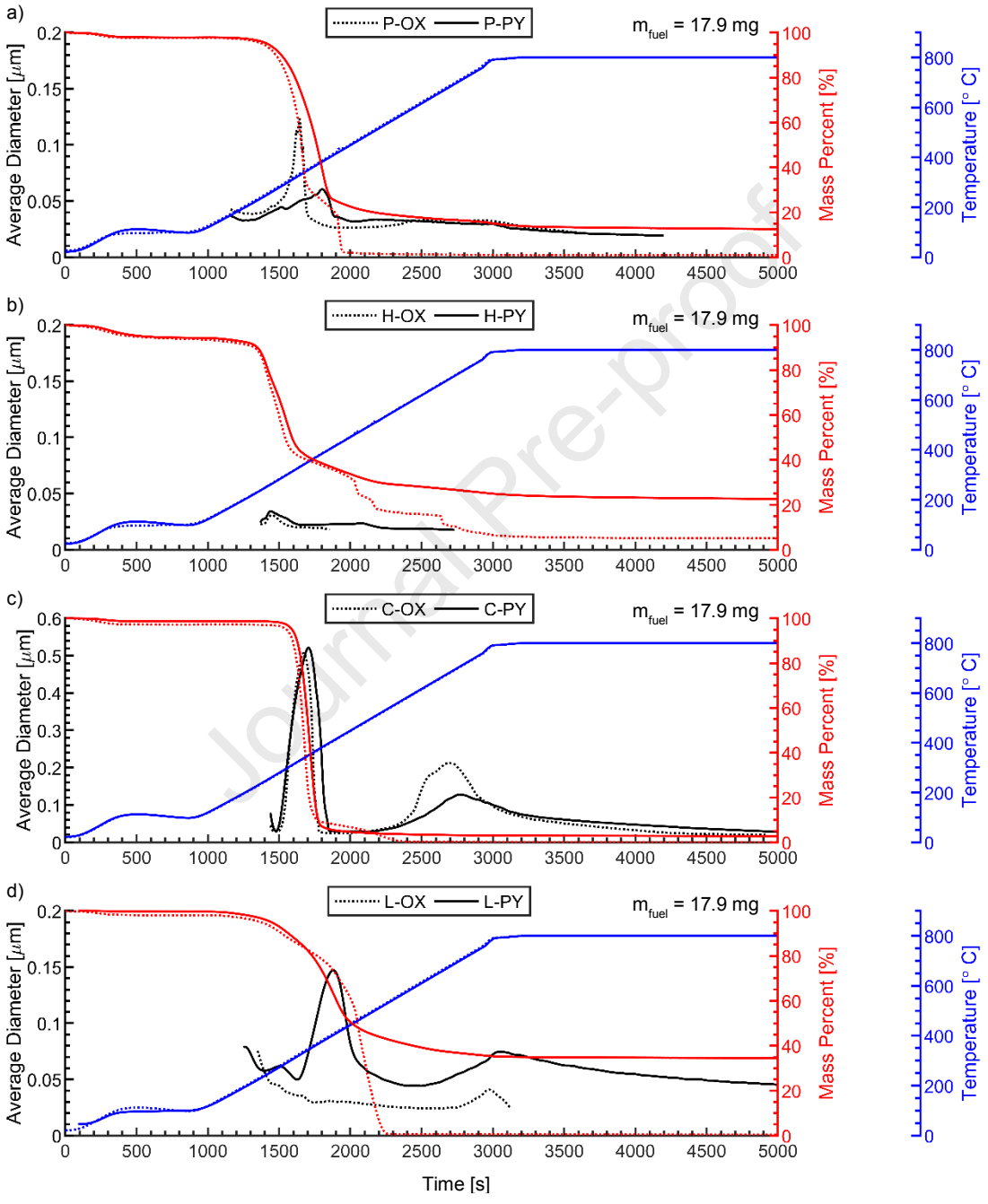

Figure 10. Mean aerodynamic aerosol diameters as a function of test time and reaction environment temperature determined for a) pinewood (P), b) hemicellulose (H), c) cellulose (C), and d) lignin (L) in 0 vol% (PY) and 21 vol% (OX) O_2 environments.

4. Conclusions

The influences of environment oxygen level, fuel mass, and fuel consumption rate on the size and quantity of aerosols produced from pyrolysis and combustion of pulverized pinewood and major lignocellulosic biomass constituents were investigated in a controlled laboratory setting, and insights into the mechanisms influencing aerosol formation in biomass burning events were achieved. Increased oxygen level was observed to decrease the total number and mass emission factors of pinewood and also increase aerosol growth. Increased fuel mass was observed to decrease the total number emission factor in both the inert and oxidative environments while nearly conserving and slightly increasing the total mass emission factor in the inert and oxidative environments, respectively, indicating oxidation and consumption of particle precursors in oxidative environments, and the consumption of smaller particles via particle coagulation and growth. The influence of combustion chemistry and particle precursor species oxidation were revealed to significantly influence aerosol emissions, and fuel heating rate, which can be imposed in an inert environment or result from thermal feedback during combustion, was found to positively correlate with fuel consumption rate and the size of aerosols produced during pyrolysis and combustion. Aerosol emissions showed insensitivity to m_{fuel}: $\dot{V}_{dilution}$ and associated parameters, and results suggest that aerosol formation, growth, and coagulation occur rapidly in the TGA and sample line upstream of dilution. The measured aerosol emissions from the major lignocellulosic biomass constituents were used to test a summative model to predict pinewood

emissions based on constituent emissions and the mass fraction of each constituent in the biomass. The simulated total number emission factors agreed within an average of 38% and 56% of the experimental values in a 0 and 21 vol% O_2 environment, respectively, and the simulated total mass emission factors agreed within an average of 330% and 56% of the experimental values in a 0 and 21 vol% O_2 environment, respectively. The importance of selecting representative lignocellulosic biomass constituents was highlighted for the summative model, specifically regarding the choice of lignin. Overall, the usefulness of the model in predicting near-source, minimally diluted emissions from dry pulverized biomass burning in relatively homogenous reaction zones was realized. This work provides new insights into the influences of oxygen level, fuel mass, and fuel consumption rate on biomass burning aerosol emissions, and provides a building block towards a fundamental approach to aerosol emission prediction for biomass pyrolysis and oxidation.

Acknowledgments

The contributions of Dr. Ed Wolfrum from the National Renewable Energy Laboratory (NREL) in Golden, CO to this work are gratefully acknowledged here.

Funding Sources

This work was supported by the National Science Foundation Graduate Research Fellowship Award #1650114 and the National Science Foundation Award #1847498.

References

Abuelnuor, A., Wahid, M., Hosseini, S., Saat, A., Saqr, K. M., Sait, H. H., & Osman, M. (2014). Characteristics of biomass in flameless combustion: A review. *Renewable and Sustainable Energy Reviews*, *33*, 363–370. https://doi.org/10.1016/j.rser.2014.01.079

Adam, E., Mutanga, O., & Rugege, D. (2010). Multispectral and hyperspectral remote sensing for identification and mapping of wetland vegetation: A review. *Wetlands Ecology and Management*, *18*(3), 281–296. https://doi.org/10.1007/s11273-009-9169-z

Andreae, M. O., & Merlet, P. (2001). Emission of trace gases and aerosols from biomass burning. *Global Biogeochemical Cycles*, *15*(4), 955–966. http://dx.doi.org/10.1029/2000GB001382

Bond, T. C., Streets, D. G., Yarber, K. F., Nelson, S. M., Woo, J. H., & Klimont, Z. (2004). A technology-based global inventory of black and organic carbon emissions from combustion. *Journal of Geophysical Research: Atmospheres*, *109*(14), 1–43. https://doi.org/10.1029/2003JD003697

Buranov, A. U., & Mazza, G. (2008). Lignin in straw of herbaceous crops. *Industrial Crops and Products*, *28*(3), 237–259. https://doi.org/10.1016/j.indcrop.2008.03.008

Cai, J., He, Y., Yu, X., Banks, S. W., Yang, Y., Zhang, X., Yu, Y., Liu, R., & Bridgwater, A. V. (2017). Review of physicochemical properties and analytical characterization of lignocellulosic biomass. *Renewable and Sustainable Energy Reviews*, *76*(October 2016), 309–322. https://doi.org/10.1016/j.rser.2017.03.072

Cao, L. M., Huang, X. F., Wang, C., Zhu, Q., & He, L. Y. (2019). Characterization of submicron aerosol volatility in the regional atmosphere in Southern China. *Chemosphere*, *236*, 124383. https://doi.org/10.1016/j.chemosphere.2019.124383

Carrier, M., Loppinet-Serani, A., Denux, D., Lasnier, J. M., Ham-Pichavant, F., Cansell, F., & Aymonier, C. (2011). Thermogravimetric analysis as a new method to determine the lignocellulosic composition of biomass. *Biomass and Bioenergy*, *35*(1), 298–307. https://doi.org/10.1016/j.biombioe.2010.08.067

Chen, J., Li, C., Ristovski, Z., Milic, A., Gu, Y., Islam, M. S., Wang, S., Hao, J., Zhang, H., He, C., Guo, H., Fu, H., Miljevic, B., Morawska, L., Thai, P., LAM, Y. F., Pereira, G., Ding, A., Huang, X., & Dumka, U. C. (2017). A review of biomass burning: Emissions and impacts on air quality, health and climate in China. *Science of the Total Environment*, *579*(November 2016), 1000–1034. https://doi.org/10.1016/j.scitotenv.2016.11.025

Chu, H., Han, W., Cao, W., Tao, C., Raza, M., & Chen, L. (2019). Experimental investigation of soot morphology and primary particle size along axial and radial direction of an ethylene diffusion flame via electron microscopy. *Journal of the Energy Institute*, *92*(5), 1294–1302. https://doi.org/10.1016/j.joei.2018.10.005

Collier, S., Zhou, S., Onasch, T. B., Jaffe, D. A., Kleinman, L., Sedlacek, A. J., Briggs, N. L., Hee, J., Fortner, E., Shilling, J. E., Worsnop, D., Yokelson, R. J., Parworth, C., Ge, X., Xu, J., Butterfield, Z., Chand, D., Dubey, M. K., Pekour, M. S., … Zhang, Q. (2016). Regional Influence of Aerosol Emissions from Wildfires Driven by Combustion Efficiency: Insights from the BBOP Campaign. *Environmental Science and Technology*, *50*(16), 8613–8622. https://doi.org/10.1021/acs.est.6b01617

Dorge, S., Jeguirim, M., & Trouvé, G. (2011). Thermal degradation of Miscanthus pellets: Kinetics and aerosols characterization. *Waste and Biomass Valorization*, *2*(2), 149–155. https://doi.org/10.1007/s12649-010-9060-4

Fang, J., Leavey, A., & Biswas, P. (2014). Controlled studies on aerosol formation during

biomass pyrolysis in a flat flame reactor. *Fuel*, *116*, 350–357. https://doi.org/10.1016/j.fuel.2013.08.002

Fitzpatrick, E. M., Ross, A. B., Bates, J., Andrews, G., Jones, J. M., Phylaktou, H., Pourkashanian, M., & Williams, A. (2007). Emission of oxygenated species from the combustion of pine wood and its relation to soot formation. *Process Safety and Environmental Protection*, *85*(5 B), 430–440. https://doi.org/10.1205/psep07020

Formenti, P., Elbert, W., Maenhaut, W., Haywood, J., Osborne, S., & Andreae, M. O. (2003). Inorganic and carbonaceous aerosols during the Southern African Regional Science Initiative (SAFARI 2000) experiment: Chemical characteristics, physical properties, and emission data or smoke from African biomass burning. *Journal of Geophysical Research D: Atmospheres*, *108*(13), 1–16. https://doi.org/10.1029/2002jd002408

Glassman, I. (1979). Phenomenological Models of Soot Processes in Combustion Systems. *Princeton Univ Nj Dept of Mechanical and Aerospace Engineering*.

Grandesso, E., Gullett, B., Touati, A., & Tabor, D. (2011). Effect of moisture, charge size, and chlorine concentration on PCDD/F emissions from simulated open burning of forest biomass. *Environmental Science and Technology*, *45*(9), 3887–3894. https://doi.org/10.1021/es103686t

Haghighi Mood, S., Hossein Golfeshan, A., Tabatabaei, M., Salehi Jouzani, G., Najafi, G. H., Gholami, M., & Ardjmand, M. (2013). Lignocellulosic biomass to bioethanol, a comprehensive review with a focus on pretreatment. *Renewable and Sustainable Energy Reviews*, *27*, 77–93. https://doi.org/10.1016/j.rser.2013.06.033

Hays, M. D., Geron, C. D., Linna, K. J., Smith, N. D., & Schauer, J. J. (2002). Speciation of Gas-Phase and Fine Particle Emissions from Burning of Foliar Fuels. *Environmental Science and Technology*, *36*(11), 2281–2295. https://doi.org/10.1021/es0111683

Hodshire, A. L., Bian, Q., Ramnarine, E., Lonsdale, C. R., Alvarado, M. J., Kreidenweis, S. M., Jathar, S. H., & Pierce, J. R. (2019). More Than Emissions and Chemistry: Fire Size, Dilution, and Background Aerosol Also Greatly Influence Near-Field Biomass Burning Aerosol Aging. *Journal of Geophysical Research: Atmospheres*, *124*(10), 5589–5611. https://doi.org/10.1029/2018JD029674

Ichoku, C., & Kaufman, Y. J. (2005). A method to derive smoke emission rates from MODIS fire radiative energy measurements. *IEEE Transactions on Geoscience and Remote Sensing*, *43*(11), 2636–2649. https://doi.org/10.1109/TGRS.2005.857328

Jolleys, M. D., Coe, H., McFiggans, G., Capes, G., Allan, J. D., Crosier, J., Williams, P. I., Allen, G., Bower, K. N., Jimenez, J. L., Russell, L. M., Grutter, M., & Baumgardner, D. (2012). Characterizing the aging of biomass burning organic aerosol by use of mixing ratios: A meta-analysis of four regions. *Environmental Science and Technology*, *46*(24), 13093–13102. https://doi.org/10.1021/es302386v

Jolleys, M. D., Coe, H., McFiggans, G., McMeeking, G. R., Lee, T., Kreidenweis, S. M., Jr., J. L. C., & Sullivan, A. P. (2014). Organic aerosol emission ratios from the laboratory

combustion of biomass fuels. *Journal of Geophysical Research: Atmospheres*, 850–871. https://doi.org/10.1002/2014JD021589

Kan, T., Strezov, V., & Evans, T. J. (2016). Lignocellulosic biomass pyrolysis: A review of product properties and effects of pyrolysis parameters. *Renewable and Sustainable Energy Reviews*, *57*, 1126–1140. https://doi.org/10.1016/j.rser.2015.12.185

Kroll, J. H., & Seinfeld, J. H. (2008). Chemistry of secondary organic aerosol: Formation and evolution of low-volatility organics in the atmosphere. *Atmospheric Environment*, *42*(16), 3593–3624. https://doi.org/10.1016/j.atmosenv.2008.01.003

Lee, W. C., & Kuan, W. C. (2015). Miscanthus as cellulosic biomass for bioethanol production. *Biotechnology Journal*, *10*(6), 840–854. https://doi.org/10.1002/biot.201400704

Liu, Y., Goodrick, S., & Heilman, W. (2014). Wildland fire emissions, carbon, and climate: Wildfire-climate interactions. *Forest Ecology and Management*, *317*, 80–96. https://doi.org/10.1016/j.foreco.2013.02.020

López-García, M., Lodeiro, P., Herrero, R., Barriada, J. L., Rey-Castro, C., David, C., & Sastre de Vicente, M. E. (2013). Experimental evidences for a new model in the description of the adsorption-coupled reduction of Cr(VI) by protonated banana skin. *Bioresource Technology*, *139*, 181–189. https://doi.org/10.1016/j.biortech.2013.04.044

May, A. A., Levin, E. J. T., Hennigan, C. J., Riipinen, I., Lee, T., Collett, J. L., Jimenez, J. L., Kreidenweis, S. M., & Robinson, A. L. (2013). Gas-particle partitioning of primary organic aerosol emissions: 3. Biomass burning. *Journal of Geophysical Research Atmospheres*, *118*(19), 11,327-11,338. https://doi.org/10.1002/jgrd.50828

May, A. A., McMeeking, G. R., Lee, T., Taylor, J. W., Craven, J. S., Burling, I., Sullivan, A. ., Akagi, S., Collett, J. L., Flynn, M., Coe, H., Urbanski, S. P., Seinfeld, J. H., Yokelson, R. J., & Kreidenweis, S. M. (2014). Aerosol emissions from prescribed fires in the United States: A synthesis of laboratory and aircraft measurements. *Journal of Geophysical Research*, *3*, 180–198. https://doi.org/10.1002/2014JD021848.Received

McLaughlin, L. P., & Belmont, E. L. (2021). Size-resolved aerosol emissions from lignocellulosic biomass and biomass constituent pyrolysis under variable dilution temperatures. *Journal of Aerosol Science*, *151*(September 2020), 105679. https://doi.org/10.1016/j.jaerosci.2020.105679

Mitchell, R. E., Sarofim, A. F., & Clomburg, L. A. (1980). Experimental and numerical investigation of confined laminar diffusion flames. *Combustion and Flame*, *37*(C), 227–244. https://doi.org/10.1016/0010-2180(80)90092-9

Mochida, M., & Kawamura, K. (2004). Hygroscopic properties of levoglucosan and related organic compounds characteristic to biomass burning aerosol particles. *Journal of Geophysical Research D: Atmospheres*, *109*(21), 1–8. https://doi.org/10.1029/2004JD004962

Muala, A., Rankin, G., Sehlstedt, M., Unosson, J., Bosson, J. A., Behndig, A., Pourazar, J.,

Nyström, R., Pettersson, E., Bergvall, C., Westerholm, R., Jalava, P. I., Happo, M. S., Uski, O., Hirvonen, M. R., Kelly, F. J., Mudway, I. S., Blomberg, A., Boman, C., & Sandström, T. (2015). Acute exposure to wood smoke from incomplete combustion - indications of cytotoxicity. *Particle and Fibre Toxicology*, *12*(1), 1–14. https://doi.org/10.1186/s12989-015-0111-7

Orasche, J., Schnelle-Kreis, J., Schön, C., Hartmann, H., Ruppert, H., Arteaga-Salas, J. M., & Zimmermann, R. (2013). Comparison of emissions from wood combustion. Part 2: Impact of combustion conditions on emission factors and characteristics of particle-bound organic species and polycyclic aromatic hydrocarbon (PAH)-related toxicological potential. *Energy and Fuels*, *27*(3), 1482–1491. https://doi.org/10.1021/ef301506h

Pardo, M., Li, C., He, Q., Levin-Zaidman, S., Tsoory, M., Yu, Q., Wang, X., & Rudich, Y. (2020). Mechanisms of lung toxicity induced by biomass burning aerosols. *Particle and Fibre Toxicology*, *17*(1), 1–15. https://doi.org/10.1186/s12989-020-0337-x

Petters, M. D., Carrico, C. M., Kreidenweis, S. M., Prenni, A. J., DeMott, P. J., Collett, J. L., & Moosmüller, H. (2009). Cloud condensation nucleation activity of biomass burning aerosol. *Journal of Geophysical Research Atmospheres*, *114*(22), 1–16. https://doi.org/10.1029/2009JD012353

Qu, T., Guo, W., Shen, L., Xiao, J., & Zhao, K. (2011). Experimental study of biomass pyrolysis based on three major components: Hemicellulose, cellulose, and lignin. *Industrial and Engineering Chemistry Research*, *50*(18), 10424–10433. https://doi.org/10.1021/ie1025453

Ramnarine, E., Kodros, J. K., Hodshire, A. L., Lonsdale, C. R., Alvarado, M. J., & Pierce, J. R. (2019). Effects of near-source coagulation of biomass burning aerosols on global predictions of aerosol size distributions and implications for aerosol radiative effects. *Atmospheric Chemistry and Physics*, *19*(9), 6561–6577. https://doi.org/10.5194/acp-19-6561-2019

Reid, J. S., Eck, T. F., Christopher, S. A., Koppmann, R., Dubovik, O., Eleuterio, D. P., Holben, B. N., & Reid, E. A. (2005). A review of biomass burning emissions part III : intensive optical properties of biomass burning particles. *Atmospheric Chemistry and Physics*, 827–849. https://doi.org/https://doi.org/10.5194/acp-5-827-2005

Reid, J. S., Koppmann, R., Eck, T. F., Eleuterio, D. P., Division, M., Juelich, F., & County, B. (2005). A review of biomass burning emissions part II : intensive physical properties of biomass burning particles. *Atmospheric Chemistry and Physics*, *5*, 799–825. https://doi.org/10.5194/acp-5-799-2005

Rissler, J., Vestin, A., Swietlicki, E., Fisch, G., Zhou, J., Artaxo, P., & Andreae, M. O. (2006). Size distribution and hygroscopic properties of aerosol particles from dry-season biomass burning in Amazonia. *Atmospheric Chemistry and Physics*, *6*(2), 471–491. https://doi.org/10.5194/acp-6-471-2006

Sakamoto, K. M., Laing, J. R., Stevens, R. G., Jaffe, D. A., & Pierce, J. R. (2016). The evolution of biomass-burning aerosol size distributions due to coagulation: Dependence on fire and meteorological details and parameterization. *Atmospheric Chemistry and Physics*, *16*(12),

7709–7724. https://doi.org/10.5194/acp-16-7709-2016

Shen, G., Xue, M., Wei, S., Chen, Y., Wang, B., Wang, R., Shen, H., Li, W., Zhang, Y., Huang, Y., Chen, H., Wei, W., Zhao, Q., Li, B., Wu, H., & Tao, S. (2013). Influence of fuel mass load, oxygen supply and burning rate on emission factor and size distribution of carbonaceous particulate matter from indoor corn straw burning. *Journal of Environmental Sciences (China)*, *25*(3), 511–519. https://doi.org/10.1016/S1001-0742(12)60191-0

Sutherland, R. A., & Khanna, R. K. (1991). Optical properties of organic-based aerosols produced by burning vegetation. *Aerosol Science and Technology*, *14*(3), 331–342. https://doi.org/10.1080/02786829108959495

Takahashi, F., & Glassman, I. (1984). Sooting Correlations for Premixed Flames. *Combustion Science and Technology*, *37*(1–2), 1–19. https://doi.org/10.1080/00102208408923743

Vose, J. M., Swank, W. T., Geron, C. D., & Major, A. E. (1996). *Biomass Burning and Global Change Volume 2 Biomass Burning in South America , Southeast Asia , and Temperate and Boreal Ecosystems , and the Oil Fires of Kuwait* (Vol. 2, pp. 733–749). The MIT Press.

Ward, D. E., & Radke, L. F. (1993). Emissions Measurements from Vegetation Fires : A Comparative Evaluation of Methods and Results, Fire in the Environment: The Ecological, Atmospheric, and Climatic Importance of Vegetation Fires, edited by: *Crutzen, P. J. and Goldammer, J. G., JohnWiley, New York*, 53–76.

Wey, C., Powell, E. A., & Jagoda, J. I. (1984). The Effect of Temperature on the Sooting Behavior of Laminar Diffusion Flames. *Combustion Science and Technology*, *41*(3–4), 173–190. https://doi.org/10.1080/00102208408923828

Wey, C., Powell, E. A., & Jagoda, J. I. (1985). The effect on soot formation of oxygen in the fuel of a diffusion flame. *Symposium (International) on Combustion*, *20*(1), 1017–1024. https://doi.org/10.1016/S0082-0784(85)80591-9

Wooster, M. J., Roberts, G., Perry, G. L. W., & Kaufman, Y. J. (2005). Retrieval of biomass combustion rates and totals from fire radiative power observations: FRP derivation and calibration relationships between biomass consumption and fire radiative energy release. *Journal of Geophysical Research Atmospheres*, *110*(24), 1–24. https://doi.org/10.1029/2005JD006318

Xie, Y., Sha, Z., & Yu, M. (2008). Remote sensing imagery in vegetation mapping: a review. *Journal of Plant Ecology*, *1*(1), 9–23. https://doi.org/10.1093/jpe/rtm005

Zhou, S., Collier, S., Jaffe, D. A., Briggs, N. L., Hee, J., Sedlacek III, A. J., Kleinman, L., Onasch, T. B., & Zhang, Q. (2017). Regional influence of wildfires on aerosol chemistry in the western US and insights into atmospheric aging of biomass burning organic aerosol. *Atmospheric Chemistry and Physics*, *17*(3), 2477–2493. https://doi.org/10.5194/acp-17-2477-2017

Highlights

- Biomass burning number and mass emission factors decrease as oxygen levels increase
- Nearly constant total mass emission factors across orders of magnitude of fuel mass
- Increased aerosol size attributed to combustion chemistry and fuel consumption rate
- Summative model predicts biomass pyrolysis and oxidation emissions well
- Cellulose highlighted as a significant aerosol contributor during biomass burning

Declaration of interests

☒ The authors declare that they have no known competing financial interests or personal relationships that could have appeared to influence the work reported in this paper.

☐The authors declare the following financial interests/personal relationships which may be considered as potential competing interests: